8900–8922 *Nucleic Acids Research, 2021, Vol. 49, No. 15* *Published online 9 August 2021*
https://doi.org/10.1093/nar/gkab653

Nuclear export of plant pararetrovirus mRNAs involves the TREX complex, two viral proteins and the highly structured 5′ leader region

Julie Kubina[1,†], Angèle Geldreich[1,†], Jón Pol Gales[1,†], Nicolas Baumberger[1], Clément Bouton[1], Lyubov A. Ryabova[1], Klaus D. Grasser[2], Mario Keller[1] and Maria Dimitrova[1,*]

[1]Institut de biologie moléculaire des plantes, CNRS, Université de Strasbourg, Strasbourg, France and [2]Cell Biology & Plant Biochemistry, Biochemistry Centre, University of Regensburg, D-93053 Regensburg, Germany

Received August 01, 2020; Revised July 09, 2021; Editorial Decision July 12, 2021; Accepted July 22, 2021

ABSTRACT

In eukaryotes, the major nuclear export pathway for mature mRNAs uses the dimeric receptor TAP/p15, which is recruited to mRNAs via the multisubunit TREX complex, comprising the THO core and different export adaptors. Viruses that replicate in the nucleus adopt different strategies to hijack cellular export factors and achieve cytoplasmic translation of their mRNAs. No export receptors are known in plants, but Arabidopsis TREX resembles the mammalian complex, with a conserved hexameric THO core associated with ALY and UIEF proteins, as well as UAP56 and MOS11. The latter protein is an orthologue of mammalian CIP29. The nuclear export mechanism for viral mRNAs has not been described in plants. To understand this process, we investigated the export of mRNAs of the pararetrovirus CaMV in Arabidopsis and demonstrated that it is inhibited in plants deficient in ALY, MOS11 and/or TEX1. Deficiency for these factors renders plants partially resistant to CaMV infection. Two CaMV proteins, the coat protein P4 and reverse transcriptase P5, are important for nuclear export. P4 and P5 interact and colocalise in the nucleus with the cellular export factor MOS11. The highly structured 5′ leader region of 35S RNAs was identified as an export enhancing element that interacts with ALY1, ALY3 and MOS11 *in vitro*.

GRAPHICAL ABSTRACT

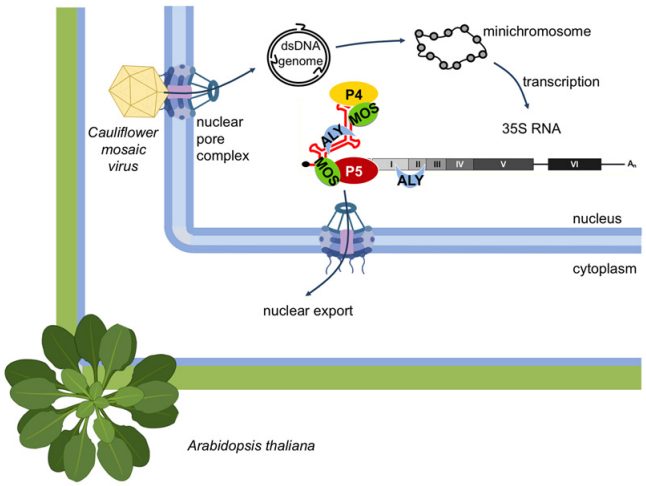

INTRODUCTION

Nuclear mRNA export is central to gene expression and has been extensively studied and documented for many years in yeast and metazoa. To be efficiently exported transcripts must undergo several maturation steps including capping (1), splicing (2) and 3′ end formation (3). During this co-transcriptional maturation, which (except for capping) occurs in the nuclear perispeckles (2), maturation and export factors are recruited to transcripts forming large messenger ribonucleoproteins (mRNPs). These factors allow mRNPs to dock with the nuclear basket of the nuclear pore complex (NPC), transit the central channel and be released from the cytoplasmic fibrils (4–6). The major transporter for mRNPs is the protein heterodimer TAP/p15 (also known

*To whom correspondence should be addressed. Tel: +33 3 67 15 53 72; Fax: +33 3 67 15 53 00; Email: m.dimitrova@unistra.fr
†The authors wish it to be known that, in their opinion, the first three authors should be regarded as joint first authors.
Present addresses:
Julie Kubina, Université de Strasbourg, INRAE, SVQV UMR-A 1131, F-68000 Colmar, France.
Clément Bouton, King's College London, Guy's Hospital, London SE1 9RT, UK.

as NXF1/NXT1 in metazoa and Mex67/Mtr2 in yeast). Although TAP can directly bind single stem-loop structures called constitutive transport elements (CTE) (7,8), in the case of spliced mRNAs, TAP is recruited by adaptor proteins rather than by direct sequence-specific RNA binding (5,9). A key player in mRNP biogenesis, maturation and TAP/p15 recruitment is the transcription and export (TREX) complex. TREX is conserved across a wide range of organisms (5). TREX-1 comprises a hexameric core called THO (10) and some important additional proteins such as the ALY adaptors (11) and their functional homologues UIF (12), UAP56 (13) and CIP29 (14). ALY and THO are rapidly recruited to nascent mRNAs by the cap-binding complex (CBC) (15–17), which associates with the 5′ cap. During splicing, exon junction complexes (EJCs) are deposited on mRNAs and additional ALY copies are then loaded upstream of the exon-exon junctions (18) or transferred from the CBC (17). The DEAD-box RNA helicase UAP56, also considered a component of the EJC (18), associates with both ALY and CIP29 in an ATP-dependent manner (19). Finally, the TREX adaptor proteins, and mostly ALY, together with the THO subcomplex, act as a binding platform for the export receptor TAP (and its associated p15 protein) (20), which directs the export-competent mRNPs to the nuclear pore (21). UAP56 and ALY are released before or during translocation through the NPC (22).

Although splicing is essential for the nuclear export of mature mRNAs, intronless or intron-retaining mRNAs can also recruit TREX components and adaptors to load the export transporters TAP/p15. In such cases the association between the CBC and TREX complex is crucial (23), as is probably the ability of the scanning spliceosomes to deposit (with lower efficiency) EJC and mRNA export factors on single-exon transcripts (17). Intronless mRNAs probably use different strategies to attract TAP/p15: histone mRNAs bind SR adaptor proteins that directly recruit TAP/p15 (24–26), whereas other intronless cellular mRNAs harbour conserved cytoplasmic accumulation regions (CARs) that interact with TREX components (27,28).

The nuclear export of mRNAs remains poorly studied in plants, where only the composition of the Arabidopsis TREX complex is well-described (29). With some minor differences, the hexameric THO subcomplex resembles that of metazoa (30). These differences may be important to allow plants to export different RNA populations and to adapt to changing environmental conditions. ALY adaptor proteins (ALY1–4) are encoded by four genes that are ubiquitously expressed in vegetative cells in Arabidopsis (31). All four ALYs localise to the nucleus, interact with UAP56, and bind to single and double-stranded RNA (32). Single and double *aly* knockout plants do not exhibit visible phenotypes. Quadruple *aly1 aly2 aly3 aly4* mutants (*4xaly*) show defects in growth, flowering and seed production, and a nuclear accumulation of mRNAs, suggesting inefficient nuclear export of mRNAs (32). Two UIF-like proteins have also been described in Arabidopsis: they bind to RNA and UAP56 and cooperate with ALY1–4 to mediate efficient nucleocytosolic mRNA transport (33). The DEAD-box RNA helicase UAP56 is encoded by two adjacent genes in Arabidopsis. The resulting identical proteins interact with single and double-stranded RNA, and with ALY and MOS11 proteins (34). MOS11 is the Arabidopsis orthologue of CIP29, also a nuclear protein; *mos11* knockout plants show nuclear accumulation of mRNAs (35). The Arabidopsis genome does not encode orthologues of TAP, the main mRNP transporter that is loaded via interactions with ALY-like adaptor proteins in yeast and metazoans. Plants may therefore use different exportins to direct and transport mRNPs through the nuclear pore (29).

Like all living organisms, yeast, plants and metazoa are exposed to diverse viral infections. Many DNA and RNA viruses with nuclear replication steps in their life cycles export viral mRNAs by hijacking the TAP/p15 pathway (36). Herpesviruses, in which most mRNAs are intronless, have evolved highly efficient mechanisms for their maturation and export. They use a conserved multifunctional viral protein (ICP27 for herpes simplex virus 1 (HSV1) or its homologue ORF57 for herpes virus saimiri and Kaposi sarcoma herpesvirus (KSHV), for example), which interacts with both viral transcripts and cellular adaptors such as ALY, UIF and CIP29, recruiting the whole TREX complex and enhancing viral mRNA accumulation and export (37–43). Simple retroviruses, such as Mason-Pfizer monkey virus (MPMV) use highly structured CTEs on their mRNAs that directly bind TAP with high affinity (44). Hepatitis B (pararetro)virus (HBV) mRNAs also harbour a structured region named the posttranscriptional regulatory element (PRE), which is necessary for TREX recruitment on intronless viral mRNAs and efficient expression of viral proteins (45).

The paraphyletic group *Pararetrovirus*, whose members replicate their circular double-stranded DNA genomes by reverse transcription, not only includes the vertebrate *Hepadnaviridae* family but also plant *Caulimoviridae*. *Caulimoviridae* together with *Geminiviridae*, *Nanoviridae* (both with circular single-stranded DNA genomes) and *Nucleorhabdoviruses* (with single-stranded negative-sense RNA genomes) induce synthesis of viral mRNAs in the nuclei of the infected plant cells. These mRNAs are then necessarily exported into the cytoplasm to be translated and to enable viral replication. In plants, the general mechanism of the nuclear export of mRNAs is poorly characterised. Moreover, nothing is known regarding how phytoviruses export viral mRNAs from the nucleus. To address this question, we investigated the nuclear export of mRNAs of *Cauliflower mosaic virus* (CaMV), the type member of the family *Caulimoviridae*.

The CaMV replication cycle includes two main steps, one in the nucleus and one in the cytoplasm: (a) Following entry into the plant cell and disassembly of the capsid proteins on the nuclear envelope (46), the viral dsDNA is imported into the nucleus, where it associates with histones to form a minichromosome that is used as a template for transcription by the host DNA-dependent RNA polymerase II (Pol II). This produces a capped and polyadenylated polycistronic pregenomic 35S RNA (pgRNA) which comprises the complete genome and encodes six major proteins (P1 to P6). Pol II transcription also produces a monocistronic subgenomic 19S RNA encoding a single protein, P6 (47). Although splicing rarely occurs for plant viruses, about 70% of the total CaMV 35S RNA undergoes

alternative splicing, which generates four spliced isoforms and involves four splice donor sites and a single splice acceptor site (48). Alternative splicing appears to be a conserved and complex phenomenon since upon inactivation of splice sites by mutagenesis it is rescued by the activation of numerous cryptic splice donor and acceptor sites, highlighting the key role of this process in CaMV biology (49). (b) All these different mRNA isoforms are then exported to the cytoplasm, where their translation and the reverse transcription of pgRNA occur. The six viral proteins are as follows: the P1 movement protein; the P2 aphid transmission factor; the P3 capsid-associated protein; the P4 coat protein; the P5 polyprotein homologous to the retrovirus Pol protein which harbours a C-terminal reverse transcriptase/RNase H and an N-terminal aspartic proteinase that is released by self-cleavage (50); the multifunctional P6 protein which triggers, among others, the transactivation of polycistronic 35S RNA translation (51) and the formation of numerous electron-dense inclusion bodies also known as viral factories (47). The newly synthesised dsDNA is packaged into the virions to move from cell to cell and be transmitted from plant to plant.

In this study, we provide the first description of the nuclear export of mRNAs of a plant virus, CaMV. Our data demonstrate that CaMV exports its 35S polycistronic mRNAs using the TREX export complex, and that MOS11, the adaptor protein ALY and the THO component TEX1 are required for efficient 35S mRNA export in Arabidopsis. We also show that the viral capsid protein P4 and the reverse transcriptase P5 are important for viral mRNA export, that they both interact with MOS11 *in vitro* and in protoplasts, and that they both co-localise with this export factor in the nucleus. We provide evidence that the highly structured 5′ untranslated region (5′ UTR) of the 35S RNAs, also called the leader region, acts as an export enhancing element, which can load ALY1, ALY3 and MOS11 proteins *in vitro*.

MATERIALS AND METHODS

Plant material and growth

For virus infection (CaMV or TuMV) Arabidopsis (*Arabidopsis thaliana*) Col-0 was grown on soil in a growth chamber, with 12 h photoperiod at 22°C and 12 h dark at 18°C, while for protoplast preparation, plants were grown on MS medium (52). In the latter case, after sowing, seeds were stratified in darkness for at least 24h at 4°C prior to incubation in the plant growth chamber under long-day conditions (16h photoperiod at 22°C, 8 h dark at 18°C) for 10 ± 2 days.

The *CA-rop2* mutant was described in (53) and kindly provided by Z. Yang. Seeds of the *mos11-2* T-DNA insertion line (SAIL_266_E03) (35) were obtained from the Arabidopsis Biological Resource Center (ABRC) and characterized by PCR-based genotyping to distinguish between plants that are heterozygous or homozygous for the T-DNA insertion. PCR was performed on genomic DNA isolated from leaves, using the ABRC recommended primers specific for the T-DNA insertion and the target gene *mos11* (data not shown). Arabidopsis double mutant *tex1 mos11* was described in (54) while double mutants *aly1 aly2* and *aly3 aly4*, and quadruple *aly1 aly2 aly3 aly4* mutant (*4xaly*) were characterised in (32).

Viruses and host inoculation

All CaMV experiments were performed with the Cabb B-JI isolate (John Innes Institute, Norwich, GB), by mechanical inoculation of young rosette stage (4-leaf) plants with infectious Arabidopsis sap. TuMV-GFP (UKI isolate) (55) infectious sap from *Brassica napus* cv. Drakkar, was provided by Manfred Heinlein and inoculated in the same manner.

Plasmids

Details of the plasmid constructs are given in the Supplementary Data at NAR online.

Analysis of CaMV proteins and genomic DNA in infected Arabidopsis plants

Details are given in the Supplementary Data at NAR online.

Arabidopsis protoplast isolation and transfection

Protoplasts were isolated as described by (56) and adapted by Bouton (49). Briefly, 10-day-old *in vitro* grown Arabidopsis seedlings were finely chopped and incubated overnight, at 26°C under gentle shaking (50 rpm) in 25 ml enzyme solution (20 mM MES pH 7.5 – 0.4 M mannitol – 20 mM KCl – 10 mM $CaCl_2$ – 1.5% cellulase R10 – 0.4% macerozyme R10). The digestion medium was then filtrated to eliminate leaf debris, washed in 20 ml 2 mM MES pH 5.7 – 154 mM NaCl – 125 mM $CaCl_2$ – 5 mM KCl solution and gently centrifuged to remove enzymes, and protoplasts were finally suspended in 4 mM MES pH 5.7 – 0.4 M mannitol – 15 mM $MgCl_2$ medium, counted and adjusted to 10^6 protoplasts/ml.

Transfection was performed as described by (56) with modifications: 300 µl protoplasts were mixed with 300 µl 2 mM MES pH 5.7 – 0.2 M mannitol - 30% PEG4000 – 100 µM $CaCl_2$ - DNA transfection solution (10 µg expression plasmid and 10 µg carrier plasmid) and incubated during 15 min at room temperature. Transfection was stopped with 1 ml 2 mM MES pH 5.7 - 154 mM NaCl – 125 mM $CaCl_2$ – 5 mM KCl solution; protoplasts were centrifuged, suspended in 1 ml 4 mM MES pH 5.7 – 0.2 mannitol – 20 mM KCl and incubated for 20 to 26h in the dark at 23°C. The ratio of transfected fluorescent protoplasts, expressing EGFP and/or mRFP, was estimated on Axio Zoom V.16 microscope (Zeiss) at 10-fold magnification and excitation at 488 nm (EGFP), 561 nm (mRFP) and 660 nm (chlorophyll).

Subcellular fractionation of transfected Arabidopsis protoplasts

The transfected protoplasts were centrifuged 5 min at 100 × g, cell pellets were suspended in 100 µl hypotonic buffer (10 mM Tris–HCl pH 7.5, 10 mM NaCl, 0.3% NP-40) and centrifuged again 10 min at 5000 × g. 90 µl of supernatants (cytoplasmic fractions) were harvested and pellets (nuclear fractions) washed 3 times in hypotonic buffer and finally

suspended in 90 μl hypotonic buffer. Total fractions are prepared by suspending the protoplasts in 100 μl hypotonic buffer. Purity of the fractions was determined by western blot detection of nuclear histone H3 and cytoplasmic UDP-glucose pyrophosphorylase 1 (UGPase).

RNA extraction and analysis by real time RT-PCR

RNAs were extracted from total, cytoplasmic and nuclear fractions with TRI-Reagent (Sigma), applied on Phasemaker columns (Invitrogen), according to the manufacturer's instructions, and finally suspended in RNase-free water. RNAs were further treated with TURBO DNase (Invitrogen) for 30 min at 37°C and analysed by PCR to monitor digestion efficiency. cDNAs were synthesised using the same amounts of RNAs for all samples with SuperScript IV and in presence of Oligo$(dT)_{20}$ Primers and Random Hexamers, according to the manufacturer's instructions (Invitrogen).

CaMV 35S RNAs in total, cytoplasmic and nuclear fractions were quantified through their respective cDNAs, diluted to 1/20, with LightCycler™ 480 SYBR Green I Master (Roche Life Science), and 35S RNA specific primers, targeting ether the P5 coding sequence: TATAGCCCAA TGGATCGTGA (FW) and CTTCTCGGCTTCATTGTT GA (REV), producing a 126 bp amplicon (nt 4387–4493 of 35S RNA), or the P4 coding sequence, (during the P5 complementation assays): CGGTTCTGGTATAATCTG (FW) and TCTTCGGTAGTTGTCATA (REV), producing a 161 bp amplicon (nt 2831–2991 of 35S RNA). Normalisation was performed to a set of four mRNAs of cellular housekeeping genes (*TIP41* (AT4G34270), *GAPDH* (AT3G04120.1), *ACTINE 2* (AT3G18780) and *SAND* (AT2G28390)). Besides them, Ct values were also normalized to those of *GFP* and/or *mRFP* as indicators of the transfection efficiencies.

The quantification of four cellular mRNAs in Arabidopsis WT and export mutants *mos11*, *aly1 aly2*, *aly3 aly4* and *4xaly* was performed by RT-PCR with the following primers: (1) AGGTGTGGCAAGCACTTTTG (FW) and TTCGACAAAGCGAGGCAAAC (REV) for ***TOR*** (AT1G50030); (2) AAAGGCCAAGGAAGAAGC AG (FW) and TGCTTGTTCGATGCATGCAC (REV) for ***RISP*** (AT5G61200); (3) TTGGCGGTAATGTGGC TTTG (FW) and TTTCGCTGGCTTTACCTTCG (REV) for ***CHUP1*** (AT3G25690) and (4) AGTTCAGGATTC CGGCAAAC (FW) and ATCCAGTTTTCACGCCGT TC (REV) for ***PDLP1*** (AT5G43980).

Protein purification

Details are given in the Supplementary Data at NAR online.

GST pull-down assays

Using plasmids pGEX-6P1, GST and GST-MOS11 were expressed in *Escherichia coli* BL21 (DE3) and affinity captured on glutathione sepharose 4B (GE Healthcare) as described by (57). Briefly, after 4h IPTG induction at 20°C, 500 ml bacterial cultures were harvested, suspended in 30 ml 50 mM Tris–HCl pH 7.5 – 1 M NaCl – 2 mM DTT – 0.1 mM EDTA – 0.5% NP-40 – Protease Inhibitors (Roche) – 10 U RQ1 RNase-free DNase (Promega Corporation), and lysed by sonication. Soluble protein fractions, obtained after centrifugation, were incubated over night with 500 μl of 50% slurry of glutathione sepharose beads and washed 3 times with the same buffer at 150 mM NaCl. Protein capture on beads was analysed by SDS-PAGE and Coomassie Blue staining.

P3, P4, P5 and its truncated versions were *in vitro* transcribed from the T7 promoter present in pGADT7 (Clontech) and translated in the presence of 10 μCi ^{35}S-methionone in TnT T7 Coupled Reticulocyte Lysate System (Promega Corporation), according to the manufacturer's instructions.

For *in vitro* binding analyses, 50 μl of GST or GST-MOS11 proteins on glutathione- Sepharose 4B beads (50% slurry) were incubated on a rotating device with 10 μl of each *in vitro* synthesized CaMV protein in a final volume of 200 μl. The beads were then washed three times, pelleted at 500 × g for 5 min, and boiled in SDS-PAGE sample buffer. GST and GST-MOS11 bound and unbound fractions were analysed by SDS-PAGE and autoradiography.

For EMSA, affinity-bound GST-MOS11 was eluted by 10 μg GST-coupled PreScission Protease (produced and provided by Nicolas Baumberger) during 2 × 16 h at 4°C. Cleaved MOS11 was harvested in the supernatants after 5 min centrifugation at 500 × g at 4°C.

Co-immunoprecipitation assays

EGFP-P4 or EGFP-P5 and MOS11-mRFP co-transfected protoplasts were incubated in the dark for 20h at 23°C. The co-transfected protoplasts were next pelleted at 1000 × g for 5 min and lysed for 15 min at 4°C, as described by (58) (Tris–HCl 50mM, pH7.5 – NaCl 150 mM – EDTA 5 mM – DTT 1mM – Triton X-100 1% – Complete Protease Inhibitors, Roche). Cellular debris were then removed by centrifugation for 5 min at 1000 × g 4°C and the supernatants were incubated with 7 μl anti-EGFP-coated magnetic beads (kindly prepared and provided by Quentin Chevalier & Vianney Poignavent) on a rotating device for 16h at 4°C. Protein capture on the beads was analysed by SDS-PAGE and immunoblotting with rabbit polyclonal anti-EGFP (59) and mouse monoclonal anti-mRFP (Sigma Aldrich, SAB-2702214).

Fluorescence localisation analysis

Fluorescent Arabidopsis protoplasts, transfected with expression plasmids coding for EGFP, mRFP and/or proteins fused with these fluorescent proteins, were observed at 63-fold magnification between a polylysine slide and cover slip, with a silicone spacer in-between, on a Zeiss LSM780 confocal microscope (Jena, Germany). EGFP and mRFP were viewed by excitation, respectively, at 488 nm and 561 nm, with an argon laser using an appropriate emission filter to collect the green or red signal from the optical section.

EMSA

L-VII and I-II RNAs were *in vitro* produced by T7 RNA Polymerase (Thermo Scientific) from 1 μg BamHI

linearized Litmus28i, according to the manufacturer's instructions and in presence of 20 μCi [α-^{32}P]-UTP. Radiolabelled RNAs were purified by acidic phenol/chloroform treatment and isopropanol precipitation, and suspended in 50 μl RNase-free water with 20 U Ribolock RNase Inhibitor (Thermo Scientific).

Two μl (≈5000 cpm) radiolabeled RNAs were incubated for 60 min at 25°C with increasing amounts (0–20 μM) of purified ALY1-GB1-His$_6$, His$_6$-GB1-ALY3, His$_6$-GB1-EGFP or MOS11, in a final volume of 20 μl protein storage buffer. Four μl non-denaturing loading buffer 6× (30% (v/v) glycerol–0.3% bromophenol blue–0.3% xylene cyanol) were then added and protein–RNA complexes were analysed by non-denaturing 45 min gel electrophoresis at 100 V (TBE 0.5×, pH 10.5–4% (v/v) acrylamide-bisacrylamide (37.5:1)–4% glycerol (v/v)), with a 30 min pre-equilibration run at 100 V in TBE 0.5 (pH 10.5), and subsequent analysis by Amersham Typhoon Biomolecular Imager.

Luciferase assays

Fifty μl of Arabidopsis protoplast suspensions transfected in triplicate with the luciferase reporter constructs Litmus-mRFP-35S-Luc were incubated for 10 min with 50 μl Promega Bright-Glo™ Reagent (Promega). The luciferase activities were measured in duplicate in a BMG LABTECH FLUOstar® Omega plate reader, averaged and normalised to the mRFP fluorescence levels, which acted as a transfection rate control.

RESULTS

Assessment of nuclear export of CaMV 35S RNAs in Arabidopsis WT and *CA-rop2* protoplasts

To measure the 35S RNA nuclear export, we set up a protoplast transfection assay. Protoplasts were prepared from WT Arabidopsis seedlings and transfected with the 14 kbp pCaMV-GFP plasmid (60) containing an infectious CaMV genome controlled by the 35S promoter and a reporter GFP in a separate expression cassette for monitoring transfection efficiency. The detection of the different viral proteins and the newly synthesised and encapsidated viral DNA suggested that the time required for one round of replication of CaMV in transfected protoplasts is about 21 h (60).

The transfection efficiency of the 14 kbp viral genome encoding plasmid in WT Arabidopsis protoplasts was not always sufficiently high to allow accurate quantification of CaMV RNAs by real-time RT-PCR. Conversely, Arabidopsis *CA-rop2* protoplasts were systematically and reproducibly transfected with high efficiency with pCaMV-GFP. *CA-rop2* Arabidopsis express the constitutively active GTPase ROP2 (Rho-related GTPase from plants) which is closely associated with the plasma membrane (61) and was shown to control multiple developmental processes such as seed dormancy, shoot apical dominance and lateral root initiation (53).

To exclude the possibility that the active ROP2 GTPase influences the nuclear export of viral mRNAs, we compared CaMV 35S RNA nuclear export in WT and *CA-rop2* protoplasts. At 20 hours post-transfection (hpt), RNAs were isolated from the total and enriched cytoplasmic and nuclear fractions (Figure 1C), and quantified by RT-qPCR using primers targeting the P5 coding region present on all 35S RNA isoforms. As shown, no significant difference was observed in the accumulation of the total 35S RNAs (Figure 1A), or their nucleocytoplasmic partitioning (Figure 1B) in WT and *CA-rop2* protoplasts. These findings suggest that the nuclear export of mRNAs (viral and cellular, since the Ct values of the set of common housekeeping gene mRNAs used for normalisation also remained unchanged) is not affected in *CA-rop2* protoplasts.

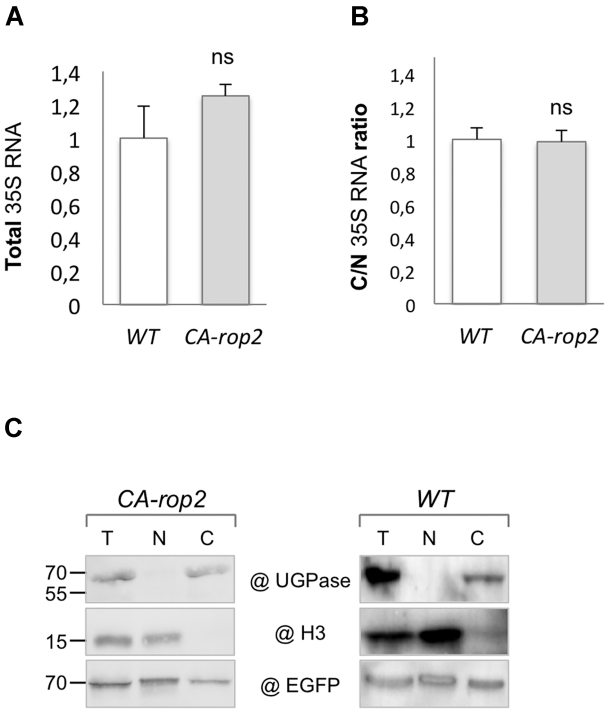

Figure 1. Total 35S RNA accumulation and nucleocytoplasmic partitioning are similar in WT and *CA-rop2* protoplasts. Leaf mesophyll protoplasts were prepared from 10-day-old WT and *CA-rop2* Arabidopsis seedlings and transfected with 10 μg pCaMV-GFP. Twenty to 26 hpt, the relative levels of 35S mRNAs were quantified in total (**A**), or nuclear and cytoplasmic fractions (**B**) by P5-specific real-time RT-PCR and normalised to a set of four cellular housekeeping genes and to GFP (as transfection indicator). Three independent experiments were performed in triplicate, each with three technical replicates. The results are expressed as the mean fold change ± SEM of the total 35S RNAs (A), or of the 35S RNA cytoplasmic-to-nuclear ratios (C/N) (B). Significance was tested with a Student's unpaired two-sample *t*-test (ns, not significant, $P > 0.05$). The purity of fractions was assessed by analysing cytoplasmic marker protein UDP-glucose pyrophosphorylase 1 (UGPase) and nuclear histone H3 by western blotting (**C**). Detection of EGFP acted as a loading control (LC).

To investigate whether not only CaMV mRNA nuclear export but also infection by CaMV occurs similarly in WT and *CA-rop2* plants, we inoculated 30 Arabidopsis plants (WT or *CA-rop2*) mechanically with CaMV. As shown in Supplementary Figure S1, after a short delay in the infection kinetics (8.3% of systemic WT versus 0% of *CA-rop2* at 14 days post-infection (dpi)), the two plant types became systemically infected at day 17 up to day 40 (97% systemic WT and 99% *CA-rop2* symptomatic plants) (Supplementary Figure S1A). They displayed the same symptoms

(typical vein-clearing and leaf-crinkling also visible on the characteristic pointed and serrated *CA-rop2* leaves) (Supplementary Figure S1B) and the same accumulation of viral proteins and genomic DNA (Supplementary Figure S1B). Viral proteins and DNA were detected only in symptomatic (S) but not in asymptomatic (A) or mock-inoculated (M) plants.

Based on the results described above, we used both WT and *CA-rop2* Arabidopsis protoplasts as controls in the following nuclear export experiments.

Arabidopsis TREX components TEX1, MOS11 and ALYs are required for nuclear export of CaMV 35S RNAs

Compared to WT Arabidopsis, homozygous *mos11*, *tex1 mos11* and *4xaly* export mutants display significant nuclear accumulation of cellular poly(A) RNAs, indicative of mRNA export defects (32,35,54). Therefore, we analysed the nuclear export of CaMV 35S RNAs in transfected protoplasts from the above mentioned mutants and in two additional ALY double mutants, *aly1 aly2* and *aly3 aly4* (32). A major difficulty was the low transfection efficiency of almost all TREX mutant protoplasts, and the fact that the nuclear export of the five reference mRNAs that we use for normalisation (4 cellular and the transfection indicator GFP) was significantly altered in the quadruple *4xaly* mutant. Therefore, Cts of 35S RNAs in *4xaly* nuclear and cytoplasmic fractions were normalised to the averaged value of all reference Cts measured in WT, *CA-rop2* and in the single and double mutants. In MOS11- but not TEX1-deficient cells, the cytoplasmic-to-nuclear ratio was reduced by half, indicating a nuclear accumulation of 35S RNAs and hence an inhibition of the nuclear export (Figure 2A). This inhibition was increased in the double mutant *mos11 tex1* (Figure 2A) and also in the ALY double mutants *aly1 aly2* and *aly3 aly4*, and especially in the quadruple *4xaly* mutant (Figure 2B). The *aly3 aly4* and *4xaly* mutants displayed almost the same level of retention of nuclear 35S RNAs, which was higher than in *aly1 aly2* suggesting that ALY3 and ALY4 are more important for the export of viral mRNAs.

We also investigated whether the accumulation of the total 35S RNAs was affected in the export mutants. As shown in Figure 2C and D, although the viral RNA levels appear increased in *mos11* and *mos11*/*tex1*, these differences are not statistically significant, indicating that the TREX export mutants have, if anything, an extremely limited effect on primary viral transcription.

Together, our data establish the essential contribution of the TREX export complex to the nuclear export of CaMV 35S RNAs.

TREX component-deficient plants are partially resistant to CaMV infection

To test whether the export inhibition of CaMV 35S RNAs observed in the Arabidopsis TREX mutants affects the viral life cycle, we studied the susceptibility to viral infection of the same TREX-deficient plants. Symptoms and virus replication kinetics (Figure 3 and Supplementary Figure S2) in 30 mechanically inoculated WT or mutant plants were compared in at least three independent experiments. In agreement with Sørensen *et al.* (54), and Pfaff *et al.* (32) we noticed that control *mos11*, double *tex1 mos11* and especially quadruple *4xaly* mutants exhibited severe phenotypic defects, with reduced leaf size and rosette diameter and elongated hypocotyls at the seedling stage (Figure 3).

In all infection experiments, the first systemic WT and *tex1* Arabidopsis were observed at 14 dpi whereas *mos11* and *tex1 mos11* plants displayed a 3-day delay: at 17 dpi only approximately 5% of the plants were systemic *versus* 36% in WT and 46% in *tex1*. Approximately 13% (*mos11*) and 16% (*tex1 mos1)* became systemic at 19 dpi when 58% of the WT and 73% of the *tex1* were already symptomatic (Figure 3A). At 26 dpi the WT/*mos11* and WT/*tex1 mos11* ratios were, respectively, 87%/35% and 87%/28%; they were 94%/48% and 94%/32% at 30 dpi and reached 99%/62% and 99%/49% at 40 dpi. As shown in Supplementary Figure S2A and B, viral proteins and genomic DNA were detected only in symptomatic but not in asymptomatic or mock-inoculated WT, *mos11* and *tex1 mos11* plants. Similar observations were made for the *tex1* mutant (data not shown). Our results show that when the nuclear export of viral mRNAs is reduced at least twofold due to the absence of MOS11 or of MOS11 and TEX1 (Figure 2A), the replication cycle of CaMV is blocked in half the inoculated plants, suggesting the importance of these components of the TREX complex for the nuclear export of viral mRNAs and the outcome of CaMV infection. Interestingly, although 35S RNA nuclear export is less efficient in the *tex1 mos11* double mutant (Figure 2A), the viral life cycle is not more severely affected in *tex1 mos11* than in *mos11* (Figure 3A).

The situation was different for the ALY adaptor mutants (Figure 3B). Compared to WT, *aly1 aly2* and *aly3 aly4* double mutants showed no delay in symptom appearance (at 14 dpi). However, the *aly1 aly2* double mutant reproducibly showed lower infection levels at 17 and 19 dpi. Infection by CaMV was severely inhibited in the *4xaly* quadruple mutant (Figure 3B), with only 20% of systemically infected plants at 40 dpi versus 92% for the WT. Among all TREX-deficient mutants, *4xaly* exhibited the most severe inhibition of the nuclear export of CaMV mRNAs (Figure 2B). Therefore, it is unsurprising that this significant nuclear retention of viral mRNAs blocked the viral life cycle in most of the inoculated plants.

Considering that the nuclear export of 35S RNAs was also strongly inhibited in *aly1 aly2* and *aly3 aly4* double mutants, although to a lesser extent than in *4xaly* (Figure 2B), one might expect that both double mutants would be less susceptible to CaMV infection. However, our results show that this is not the case, suggesting that the inhibition of viral infection in *4xaly* might be due not only to impaired viral mRNA export from the nucleus but also to a general nuclear retention of cellular mRNAs (as observed for housekeeping genes) some of which might encode host factors important for the virus.

To confirm that the partial resistance of TREX mutant Arabidopsis to CaMV infection was mainly due to the impairment of nuclear export of viral mRNAs, we first examined the susceptibility of the same TREX complex mutants to turnip mosaic virus (TuMV), a *Potyvirus* with single-stranded positive-sense RNA genome and a strictly

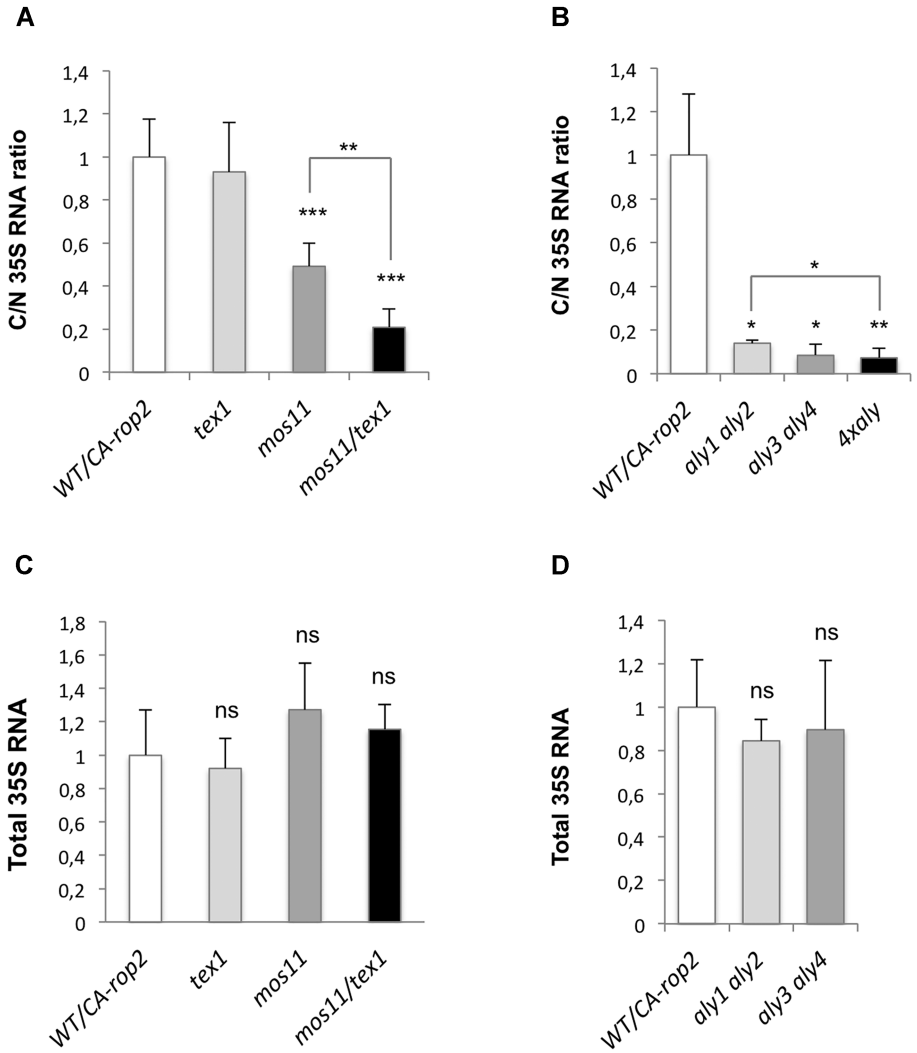

Figure 2. Nuclear export of 35S RNAs is inhibited in TREX export mutants. WT/*CA-rop2, tex1, mos11*, *tex1 mos11, aly1 aly2*, *aly3 aly4* and *4xaly* protoplasts were transfected with pCaMV-GFP. At 20 hpt, the cytoplasmic-to-nuclear ratios (**A**, **B**) or the total levels (**C**, **D**) of 35S mRNAs were determined as described in Figure 1. Cts of the cellular reference genes and of GFP, measured in WT protoplasts and the single and double mutants were averaged and used for normalisation in *4xaly*. Three independent experiments were performed in triplicate. The results are expressed as the mean fold change ± SEM. Significance was tested with a Student's unpaired two-sample t-test (ns, not significant, $P > 0.05$, * $P < 0.05$, ** $P < 0.01$, *** $P < 0.001$).

cytoplasmic replication cycle (62). For this, we used a recombinant TuMV encoding a GFP tag (TuMV-GFP) (55), the expression of which is easily followed under UV light and reflects viral replication. As shown in Supplementary Figure S3, most TuMV-GFP infections were detected at 7 dpi indifferently on WT and mutant plants. TuMV-GFP infection spread more rapidly than that of CaMV, because the maximal number of systemic plants was reached at 10 dpi for almost all WT or mutant Arabidopsis (Supplementary Figure S3).

Additionally, no significant differences were recorded in the ratios of infected plants between WT and the six assessed single, double and quadruple mutants (Supplementary Figure S3). Our results show that the TuMV-GFP replication cycle was affected in none of the TREX mutants that we tested, which is unsurprising considering that all viral RNAs here are synthesised in the cytoplasm and do not require nuclear export. However, these observations also suggest that even in the strongest export mutant, *4xaly*, the cellular mRNAs encoding host factors essential for TuMV can still be exported from the nucleus, possibly via the ALY analogue UIFs (33) or shuttling SR proteins that act as export adaptors in other organisms (5).

Finally, we also investigated in WT and TREX mutant Arabidopsis protoplasts, transfected with pCaMV-GFP, the nuclear export of four cellular mRNAs coding proteins that are either essential or important for the CaMV life cycle. We focused on three proteins that interact with the viral protein P6: TOR, whose partial depletion makes Arabidopsis resistant to CaMV (63); RISP, for which disruption of one of the two encoding genes is responsible for delayed symptom appearance and viral protein accumulation (64) and CHUP1, silencing of which results in a delay of CaMV lesion formation (65). We also analysed a protein that interacts with the viral protein P1: PDLP1, whose genetic disruption delays CaMV systemic invasion and causes milder symptoms (66).

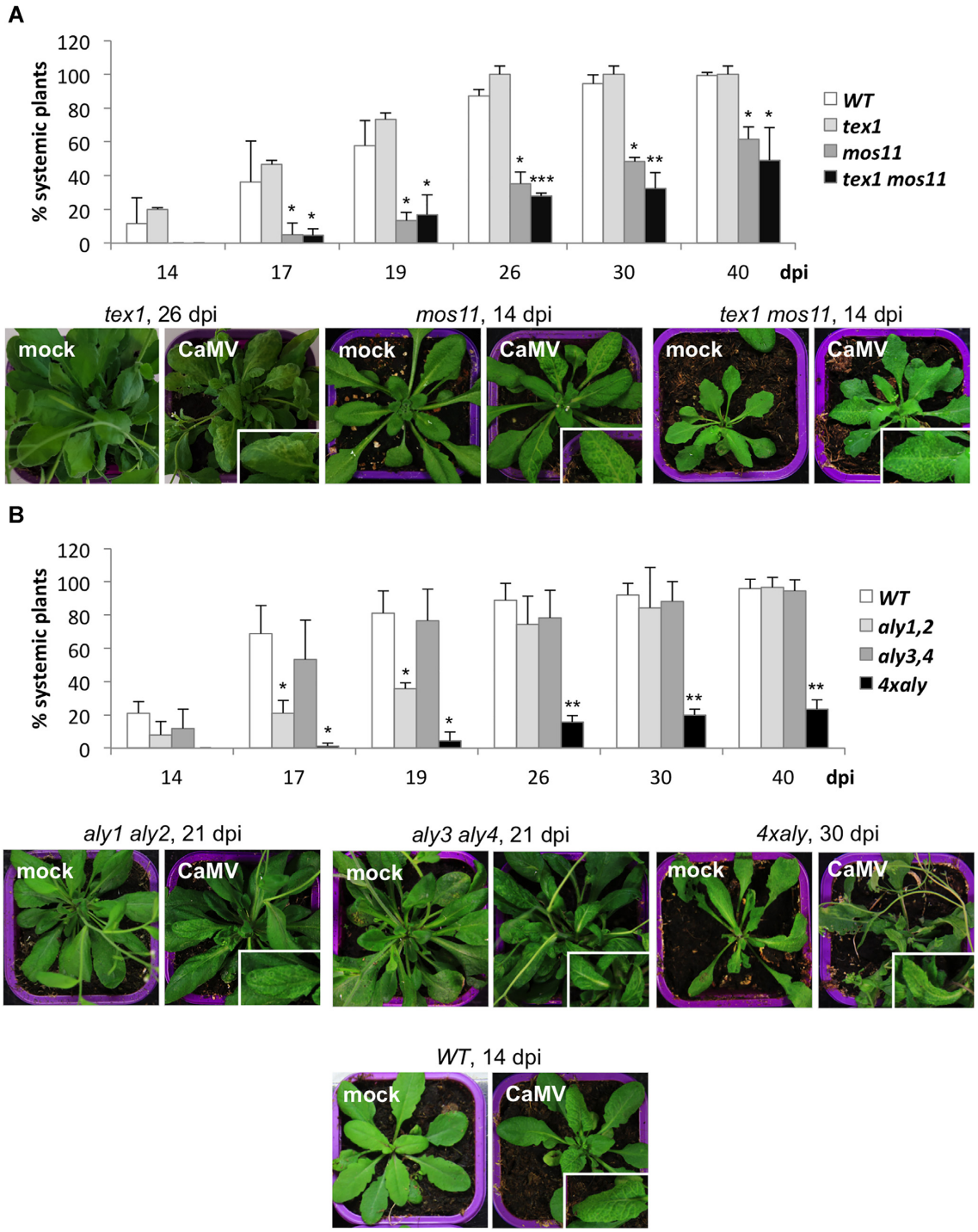

Figure 3. TREX-deficient plants are partially resistant to CaMV. (**A**) 30 WT, *tex1, mos11* and *tex1 mos11* plants and (**B**) WT, *aly1 aly2*, *aly3 aly4* and *4xaly* plants were mechanically inoculated with CaMV crude extract and monitored for symptoms. The results are means of at least three independent experiments ± SEM. Significance was tested with a Student's unpaired two-sample t-test (ns, not significant, $P > 0.05$, * $P < 0.05$, ** $P < 0.01$, *** $P < 0.001$). Representative mock- or CaMV-inoculated systemic plants with enlargement of a symptomatic leaf (on the right bottom) are shown below the corresponding histograms.

As shown in Supplementary Figure S4, despite of the differences observed in the three different experiments neither the total amounts of the above-mentioned cellular mRNAs nor their nuclear export were significantly modified in the TREX mutants compared to WT Arabidopsis, suggesting that the partial resistance of these mutant plants to CaMV infection is not due to the disrupted export of these cellular mRNAs required for the viral life cycle.

CaMV 35S RNA nuclear export depends at least on the expression of viral protein P5

To determine whether CaMV proteins are involved in the nuclear export of viral mRNAs, we mutagenised the CaMV 35S RNA-encoding plasmid (pCaMV-GFP) by creating two STOP codons in the P6 coding sequence, at positions 9 and 15. In the absence of P6, synthesised from the monocistronic 19S RNA, translation reinitiation on the polycistronic 35S RNA is completely abolished, and no viral protein can be expressed (67–70). We generated two additional mutant genomes: the pCaMV-P5/P6_STOP double mutant, in which the AUG codon at position 17 in the P5 coding sequence was also replaced by a STOP codon, and the pCaMV-P5_STOP single mutant, in which only the expression of P5 was abolished.

These plasmids were then transfected into WT/*CA-rop2* protoplasts, and the total, cytoplasmic and nuclear 35S RNAs were quantified at 20 hpt (Figure 4A). The absence of viral protein expression for the P6_STOP mutants was controlled by western blotting (Figure 4C) showing that the P4 capsid protein was detected only for pCaMV-P5_STOP and pCaMV (lanes 4 and 1) but not for pCaMV-P6_STOP (lane 2) or pCaMV-P5/P6_STOP (lane 3). As monitored in Figure 4A, in the absence of all viral proteins expression, nuclear export was strongly inhibited (pCaMV-P6_STOP, bar 2, and pCaMV-P5/P6_STOP, bar 3). An identical result was obtained when only the protease/reverse transcriptase P5, was not expressed (pCaMV-P5_STOP, bar 4), suggesting that P5 may act as a viral-specific adaptor in the nuclear export of 35S RNA. We next assessed by co-transfection experiments (Figure 4A), whether a P5 protein expressed *in trans* could restore the nuclear export and demonstrated that only a 78 kDa myc-tagged full-length protein (myc-P5_FL, bar 6 and lane 6 in Figure 4C), but neither the Nt protease domain (P5_PR, bar 7) nor the reverse transcriptase/RNase H domain (P5_RTRH, bar 8) could complement the missing viral export factor. The total amounts of 35S RNAs were not significantly different under the eight transfection and co-transfection conditions as determined by RT-qPCR with P4-specific primers, which anneal to 35S RNAs but not to the co-transfected complementing P5-encoding plasmids (Figure 4B). This observation suggests that the inhibition or complementation of the nuclear export of 35S RNAs, in the absence or presence of P5, respectively, is not due to a different RNA accumulation level.

TREX component MOS11 interacts with CaMV proteins P4 and P5

During the viral replication cycle, P5 is synthesised as an inactive 78 kDa polyprotein precursor, which progressively accumulates in the viral factories. P5 is activated there by self-cleavage by its Nt protease domain to generate a 20–22 kDa aspartic protease (PR) and a 56–58 kDa reverse transcriptase/RNase H (RTRH) (50,60,71). We therefore produced by *in vitro* translation (Figure 5A) radiolabelled full-length P5 (FL) and, according to Torruella *et al.* (50), its different functional domains: PR, RT, RH and RT/RH (RR). We also included viral proteins P3 (15 kDa) and P4 (56 kDa) and firefly luciferase (Luc, *ca.* 60 kDa) as controls. Under these *in vitro* translation conditions, P5_FL was mainly synthesised as an uncleaved polyprotein precursor, since only a ≈ 78 kDa product was detected upon autoradiography (Figure 5A, P5_FL). Larger amounts of the P5_FL (and P4) proteins synthesised *in vitro* and a longer exposure time (Supplementary Figure S5A, left panel) allow several bands of lower intensity and molecular weights to be distinguished. These could correspond to degradation products, incomplete polypeptides or other proteins endogenously produced in the rabbit reticulocyte lysates. For P5, two of these bands, indicated by asterisks (Supplementary Figure S5A, left panel), co-migrate with the RT and PR domains and could correspond to peptides cleaved by the viral PR.

The P4 capsid protein is also synthesised during viral infection as a 56 kDa precursor (pre-CP), partially processed during morphogenesis in the viral factories by the virus-encoded PR into four subspecies: p42, p39, p37 and p35, all of them lacking the Nt and/or Ct domains of pre-CP and produced in variable amounts depending on the virus preparation (46,72–74). As observed (Figure 5A), *in vitro* synthesised P4 almost co-migrates with 78 kDa P5_FL and might correspond rather to incompletely denatured dimers of the FL precursor (72,73) or to abnormally migrating monomers. We cannot exclude the possibility that this band represents dimers of shorter P4 proteins, synthesised either by initiation with an internal AUG codon or by premature translation arrest. The P4 proteins were detected using specific polyclonal antibodies, but not in the P3 and P5 translation reactions (Figure 5A, bottom).

To determine whether the viral proteins or domains produced *in vitro* interact with components of the TREX complex, we performed GST pull-down assays (Figure 5C–F) with bead-bound GST or GST-MOS11 (Figure 5B). The viral and control proteins were mostly present in the GST unbound fraction (Figure 5C) except for the RT and RH domains of P5, for which a faint signal was also detected bound to GST (Figure 5E). Luciferase control and P3 were both found exclusively in the GST-MOS11 unbound fraction, whereas P5 PR and RH domains were almost equally bound and unbound (Figure 5D, F), indicating a weak association under our assay conditions (150 mM NaCl). P4, P5_FL, P5_RT and P5_RR were enriched in the GST-MOS11-bound fraction, demonstrating that they interact with MOS11 (Figure 5F).

In the GST-MOS11-bound fraction, we detected two forms of 'full-length' P5: the *ca.* 78 kDa translation product, corresponding to the P5_FL input (Figure 5A, FL), and a second polypeptide migrating slightly higher than RT and probably comigrating with the RR doublet (a second band of extremely weak intensity was also visible on Figure 5A (**RR**)) where the electrophoresis conditions were slightly

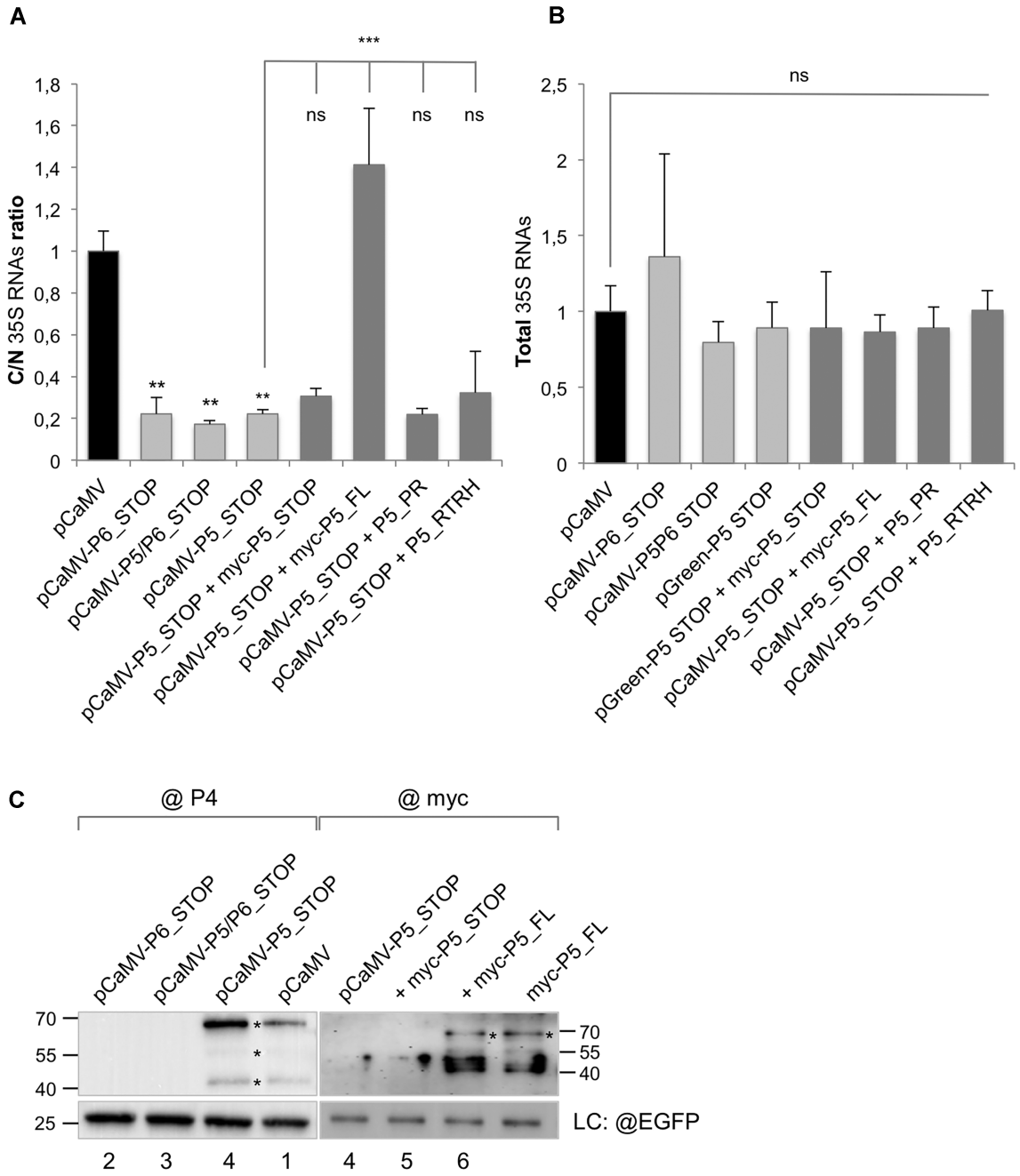

Figure 4. Nuclear export of 35S RNAs is inhibited in the absence of viral protein P5. WT/*CA-rop2* Arabidopsis protoplasts were transfected pCaMV-GFP (**1**), pCaMV-P6_STOP (**2**), pCaMV-P5/P6_STOP (**3**) or pCaMV-P5_STOP (**4**–**8**). In the three STOP plasmids (in light grey) one (for P5) or two (for P6) STOP codons were introduced after the START AUG of viral proteins P5, P6 or both. In **5** to **8** (dark grey) pCaMV-P5_STOP was co-transfected with a plasmid supplementing *in trans* with myc-P5_STOP (**5**), full-length myc-P5 (myc-P5_FL, **6**), P5 protease domain (amino acids (aa) 1–201, P5_PR, **7**) or P5 reverse transcriptase/RNase H domain (aa 202–680, P5_RTRH, **8**). At 20 hpt, the cytoplasmic-to-nuclear ratios (**A**) or the total levels (**B**) of 35S mRNAs were determined by P4-specific real-time RT-PCR and normalized to four cellular housekeeping genes, GFP (transfection indicator for pCaMV-P5_STOP) and mRFP (transfection indicator for the P5-expressing plasmids). Three independent experiments were performed in triplicate. The results are expressed as the mean fold change ± SEM of the 35S RNA cytoplasmic-to-nuclear ratios (C/N) (A) or of the total 35S RNAs (B). Significance was tested with a Student's unpaired two-samples *t*-test (ns, not significant, $P > 0.05$, ** $P < 0.01$, *** $P < 0.001$). (**C**) Detection of P4, myc-P5 and EGFP (as loading control, LC) 20 hpt by western blot with, respectively, anti-P4, anti-myc or anti-EGFP antibodies in protoplasts transfected with pCaMV-GFP (**1**), pCaMV-P6_STOP (**2**), pCaMV-P5/P6_STOP (**3**), pCaMV-P5_STOP (**4**), pCaMV-P5_STOP + myc-P5_STOP (**5**), pCaMV-P5_STOP + myc-P5_FL (**6**), or pCK-EGFP + myc-P5_FL, and corresponding, respectively, to bars 1 to 6 in (A). Positions of molecular size standards, in kilodaltons, are shown on the left and on the right. The asterisks indicate the bands corresponding to P4 and to myc-P5_FL.

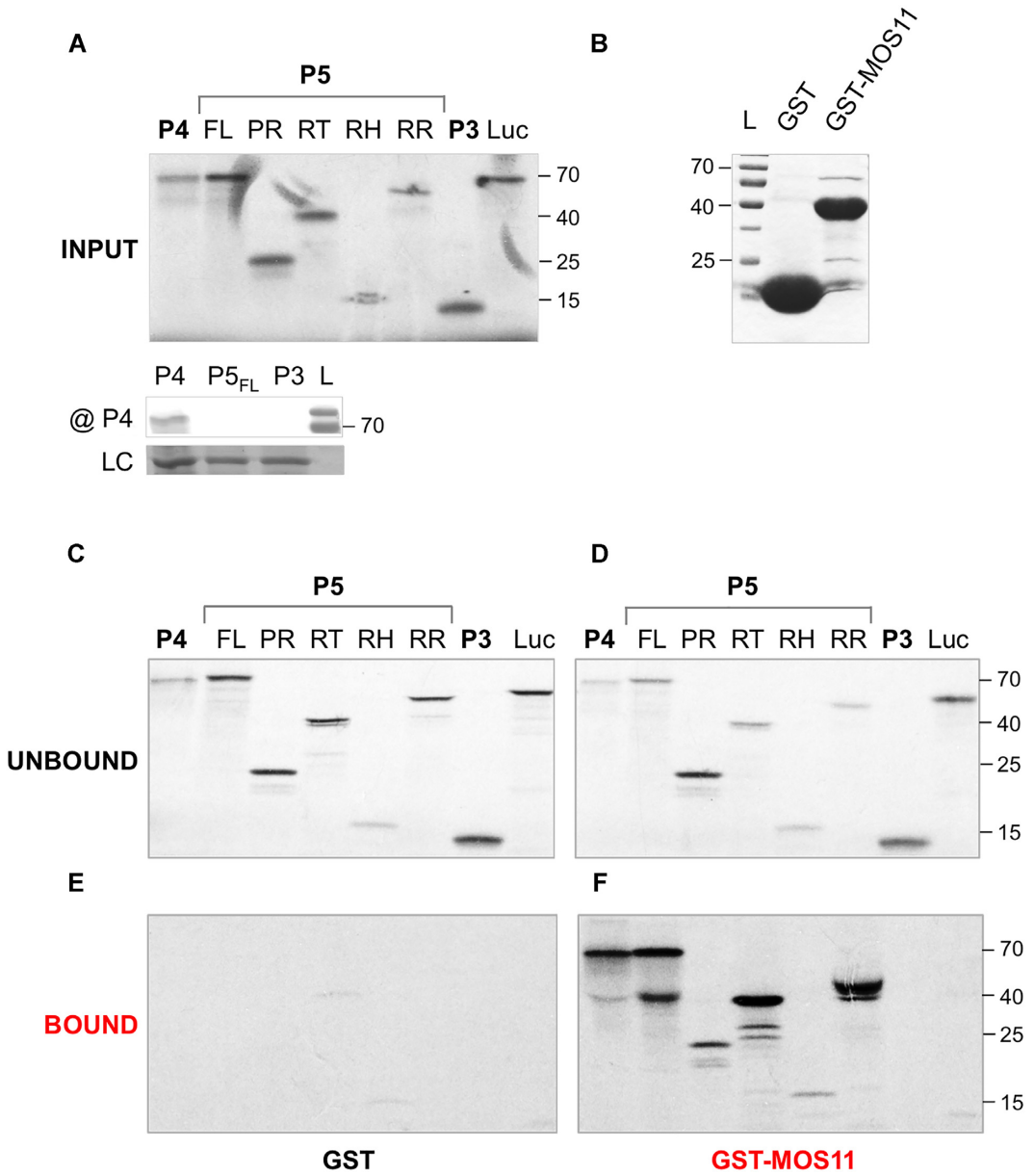

Figure 5. Viral proteins P4 and P5 interact with MOS11 *in vitro*. *In vitro* translated and [^{35}S] methionine-labelled viral proteins P3, P4 and P5 (FL: full-length, PR: protease domain (aa 1–200), RT: reverse transcriptase domain (aa 201–547), RH: RNase H domain (aa 548–680), RR: reverse transcriptase/RNase H domains (aa 201–608)) and firefly luciferase (Luc) as control (**A,** autoradiography) were incubated with bacterially expressed and glutathione bead-bound GST or GST-MOS11 (**B,** Coomassie blue staining). The inputs of P4, P5$_{FL}$ and P3 were subjected to a western blot with specific anti-P4 antibodies (A, bottom). The beads were washed and the GST- and GST-MOS11 unbound (**C, D**) and bound (**E, F**) fractions were analysed by SDS-PAGE followed by autoradiography after 24h exposure. The results are representative of four independent experiments. The inputs in (A) and (B) represent 1/9 of the amounts used in the GST pull-down assay (C–E). 1/10 of the total unbound fractions were analysed by SDS-PAGE (C, E). LC: loading control. Positions of molecular size standards, in kilodaltons, are shown on the left in (B) and on the right in (A), (D) and (F).

different). This observation was confirmed in all four GST pull-down assays we performed (with various stringency conditions, Supplementary Figure S5B, right panel), suggesting that the interaction of full-length P5 with MOS11 might activate the P5 Nt protease domain, which then partially cleaves itself but is not retained on the GST-MOS11 beads, unlike the second cleavage product generated, (RR), which can still interact with MOS11. The cleaved PR peptide was not recovered in the GST-MOS11 unbound fraction, either because the analysed amounts were insufficient to reveal its presence, or because, since it weakly interacts with MOS11, and is in competition with FL and RTRH, it was released during the extensive washing steps.

The *in vitro* interaction results indicate that two viral proteins interact with nuclear export factor MOS11: P4 and P5, *via* its RT domain. Capsid protein P4 harbours, close to its N terminus, a nuclear localisation signal (NLS), which is exposed on the surface of mature virions when the acidic N-terminus (aa 1 - 77) is deleted (46). As MOS11 displays an exclusively nuclear localisation in Arabidopsis (35,54),

one could imagine that the interaction between P4 and MOS11, observed *in vitro*, also occurs *in vivo*. However, a critical point remained concerning the apparent inability of full-length P4 to localise in the nucleus (46), necessitating further investigations. The situation of P5 was even more complex, since among all viral proteins, P5 remains the least well-characterized and its nuclear localisation has not been unambiguously confirmed, although Pfeiffer and colleagues (75) described CaMV DNA polymerase activity in infected nuclear extracts.

Both EGFP-tagged CaMV P4 and P5 proteins co-localise in cell nuclei and interact with MOS11-mRFP

We addressed the subcellular localisation of P4 and P5 by transfecting Arabidopsis protoplasts with plasmids expressing EGFP-P4 or EGFP-P5 under the control of a 35S promoter and also performed co-transfections with a MOS11-mRFP coding vector (Figure 6).

Because of its small size, EGFP (27 kDa) can enter nuclear pores; thus free EGFP is found in both the cytoplasm and nucleus in plant cells (76,77) (Figure 6B, panels 1). As illustrated in Figure 6A, EGFP-P4 displayed three main distribution patterns in transfected protoplasts: 1. forming numerous exclusively cytoplasmic aggregates of different sizes (Figure 6A, line 4) as described by Karsies *et al.* (46) for uncleaved P4 precursor; 2. forming one or several cytoplasmic aggregates but also slightly accumulating in the nucleus (6A, line 1); 3. forming cytoplasmic aggregates and strongly accumulating in the nucleus (6A, lines 3 and 4). Under co-expression conditions with strictly nuclear MOS11-mRFP (6B, panels 1; 6D, line 2) the subpopulations of EGFP-P4 forming only cytoplasmic aggregates did not move to co-localise with MOS11-mRFP (Figure 6B, panels 4). Conversely, those significantly accumulating in the nucleus merged with MOS11-mRFP but also remained as cytoplasmic aggregates (6B, panels 2 and 3).

To confirm that the observed green nuclear fluorescence was due to the fusion protein EGFP-P4 and not to cleaved EGFP, we performed fractionation experiments and western blotting with anti-EGFP polyclonal antibodies with the cytoplasmic and nuclear fractions of the transfected protoplasts (Figure 6E, left panel). As shown, three forms of EGFP-P4 of approximately 60, 80 and more than 100 kDa, were detected in both fractions. Similar observations have been described for untagged P4 expressed *in vitro* and during viral infection (e.g. 50,74,78). In our case, the uppermost form probably corresponds to P4 dimers, also detected *in vitro* (Figure 5A), whereas the middle and lower forms probably correspond, respectively, to the precursor and a processed protein. P4, which is in fusion at its N-terminus with EGFP, was probably processed at its C-terminus by cellular proteases (74); the fluorescent tag must remain part of the fusion protein since it allowed its detection.

Our combined results suggest that full-length P4, as expressed fused to EGFP, probably exists in two forms: a cytoplasmic subpopulation forming aggregates, which correlates with its primary role of self-associating capsid protein, and a second, 'soluble' subpopulation which shows a more diffuse localisation pattern and can enter the cell nucleus where it may interact with the nuclear export factor MOS11, as it does *in vitro*.

Studying the subcellular localisation of P5 was also exciting since minimal information is available about this viral protein. Expressed in fusion with EGFP, P5 exhibited a clear nucleo-cytoplasmic distribution with several cytoplasmic aggregates (Figure 6C, line 1). Under co-expression conditions nuclear EGFP-P5 perfectly merged with MOS11-mRFP (Figure 6D, panels 1–3), suggesting that the interaction between both proteins occurs in the nucleus. Full-length EGFP-P5 was also detected by western blot in both the cytoplasmic and nuclear fractions of the transfected protoplasts (Figure 6E, middle panel).

Unlike P4, the presence of an NLS has not been described for P5. The analysis of the P5 sequence with tools predicting protein targeting to nuclei and NLSs (cNLS Mapper (79) and Localizer (80)), highlighted that two adjacent motifs in the RT domain, between amino acids 276 and 305 (I**KPS**K**S**PHMAPAFLVNNEAE**KRRGKKR**MVV) and between amino acids 308 and 339 (**K**AMN**K**ATIGDAYNLPN**K**DELLTLI**RGKK**IFSS**)** define two bipartite NLSs potentially responsible for a typical nucleocytoplasmic localisation of the harbouring protein, identical to the one we observed for EGFP-P5 (Figure 6C, D). To confirm the function of these NLSs, we used the strictly cytoplasmic 120 kDa GFP-GUS fusion protein (81) (Supplementary Figure S6A), to which we added *in cis*, between GFP and GUS, P5 predicted bipartite NLSs (either the first motif (NLS_1, aa 276–305), or the second (NLS_2, aa 308–339) or both (NLS_{1+2}, aa 276–339). Arabidopsis protoplasts were transfected with the respective constructs, together with the one encoding MOS11-mRFP that we used as a nuclear indicator (Supplementary Figure S6B). Used individually (Supplementary Figure S6C, D) or together (Supplementary Figure S6E), the two P5 putative NLSs allowed GFP-GUS to move into the nucleus, where it merged with MOS11-mRFP, in the same way as the previously described bipartite NLS of CaMV protein P6 (Supplementary Figure S6F) (81).

To provide additional evidence supporting the interactions between MOS11-mRFP and EGFP-P4 or EGFP-P5, we performed co-immunoprecipitations in the transfected protoplasts, with immunocapture of the EGFP-tagged viral proteins and controls (Figure 6F, right panels). Again, we observed the typical P4 *in vivo* expression pattern comprising three bands of > 100, >70 and > 55 kDa. Importantly, MOS11-mRFP could be co-precipitated with EGFP-P5 and EGFP-P4 but not with the controls (EGFP and mock) (Figure 6F, left panel) suggesting that the *in vitro* observed interactions also occur *ex vivo.*

The leader region of CaMV 35S RNAs is an export-enhancing element

To seek a potential *cis*-acting element on 35S RNA we performed competition assays for the nuclear export machinery between CaMV 35S RNAs and shorter RNA fragments (289 to 865 nt) corresponding to the 35S 5′ end (nt 1–3000) or to its 3′ UTR (Figure 7A).

For this purpose, Arabidopsis protoplasts were co-transfected with pCaMV-GFP and an eight-fold molar

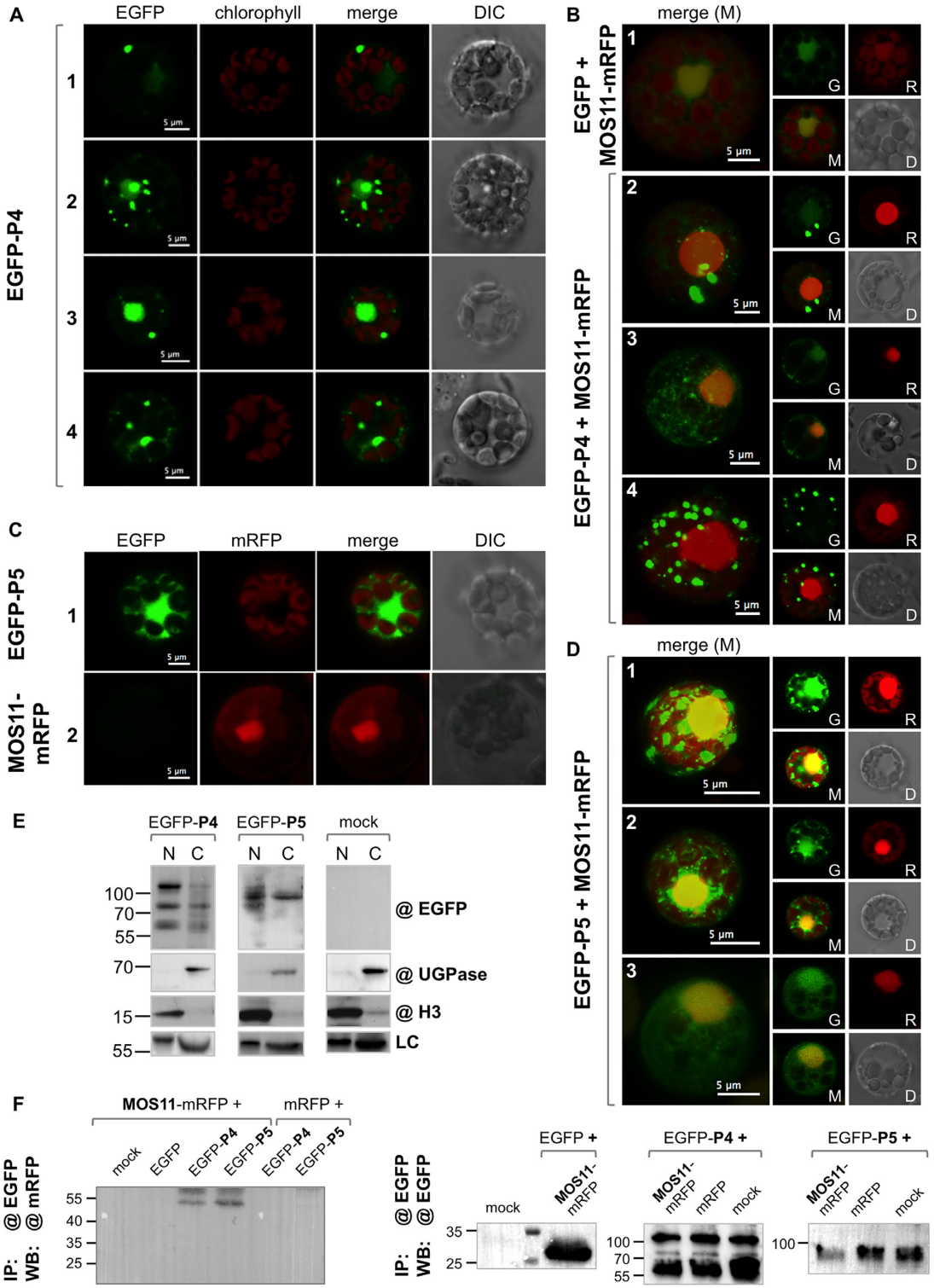

Figure 6. EGFP-P4 and EGFP-P5 both co-localise and interact with nuclear MOS11-mRFP. WT/*CA-rop2* Arabidopsis protoplasts were transfected (or co-transfected) with (**A, E**) pCK-EGFP-P4, (**B**) pCK-EGFP + Litmus-35S-MOS11-mRFP or pCK-EGFP-P4 + Litmus-35S-MOS11-mRFP, (**C, E**) pCK-EGFP-P5 (line 1) or Litmus-35S-MOS11-mRFP (line 2) and (**D**) pCK-EGFP-P5 + Litmus-35S-MOS11-mRFP. Observations of EGFP and mRFP fusion proteins were made 20 hpt by LSCM. The LSCM settings and acquisition conditions of the images were identical in all panels. In (B) and (D) panels 1 to 4, and 1 to 3, respectively are projections while all other images show single sections. G: EGFP; R: mRFP; M: merge; D: differential interference contrast (DIC) images that indicate the localisation of chloroplasts and nuclei. Scale bars: 5 µm. In (**E**) the pCK-EGFP-P4 or pCK-EGFP-P5 transfected protoplasts were subjected to nucleocytoplasmic fractionation and analysed by western blotting for the presence of full-length EGFP-P4, EGFP-P5, cytoplasmic UGPase and nuclear H3. LC: loading control. Interaction of fusion proteins EGFP-P4 and EGFP-P5 with MOS11-mRFP was analysed in transfected protoplasts by co-immunoprecipitation (**F**) with anti-EGFP magnetic beads**.** Pulled-down proteins were detected by western blot with anti-EGFP and anti-mRFP antibodies. Positions of molecular size standards in kilodaltons are shown on the left in (E) and (F).

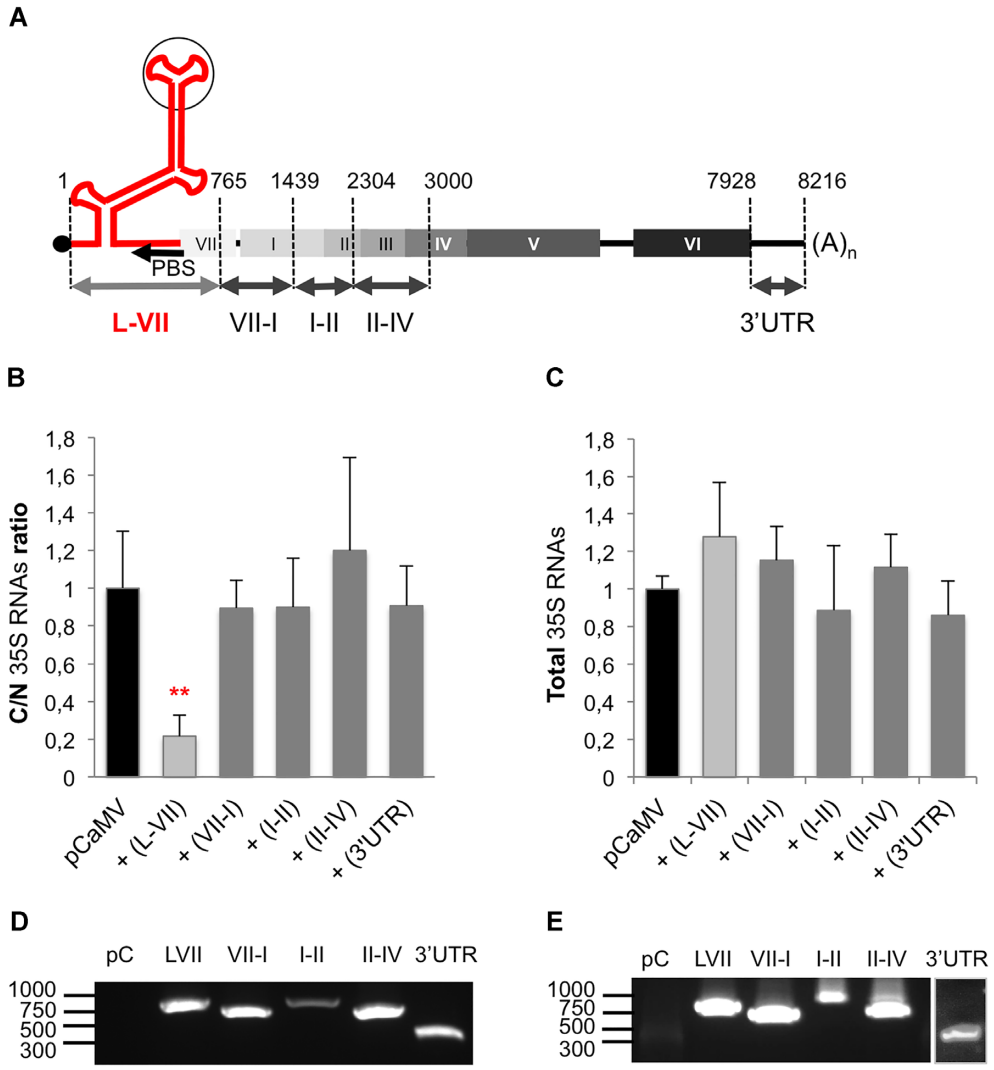

Figure 7. Co-expression of 5′UTR inhibits the nuclear export of 35S RNAs. (**A**) Structure of the capped and polyadenylated 35S RNA: the 5′ UTR (or leader (L) in red), 608 nt long, folds into a stable multibranched stem–loop (SL), and precedes the 7 ORFs (VII, I, II, III, IV, V and VI) and the 3′ UTR (nt 7,928–8,216). The five RNA fragments used in the competition assays and overlapping the leader and ORF VII (L–VII), ORF I and II (I–II), ORF II, III and IV (II–IV) and the 3′ UTR are shown with double-headed arrows. The position of the primer ($tRNA^{Meti}$) binding site (PBS, nt 596–609) is indicated by a black arrow. The coat protein P4 binding site is shown with a black circle. (**B**) to (**E**) WT/*CA-rop2* Arabidopsis protoplasts were transfected with pCaMV-GFP (black), or co-transfected with pCaMV-GFP and a 10-fold molar excess of Litmus-mRFP-35S-(L–VII) (light grey), Litmus-mRFP-35S-(I–II), Litmus-mRFP-35S-(II–IV) or Litmus-mRFP-35S-(3′UTR) (dark grey). At 20 hpt, the cytoplasmic-to-nuclear ratios (**B**) or the total levels (**C**) of 35S mRNAs were determined by P5-specific real-time RT-PCR and normalised to a set of four cellular housekeeping genes, GFP (transfection indicator for pCaMV-GFP) and mRFP (transfection indicator for the RNA fragments expressing plasmids). Three independent experiments were performed in triplicate. The results are expressed as the mean fold change ± SEM. Significance was tested with a Student's unpaired two-sample t-test (** $P < 0.01$). (**D**) Detection of the five competition RNA fragments by RT-PCR in total RNA fraction, with primers specific to their common short 5′ and 3′ sequences: (L–VII): 765 bp, (VII–I): 674 bp, (I–II): 865 bp, (II–III): 696 bp and (3′ UTR): 289 bp. (**E**) PCR positive controls, directly amplified with the same primers from the respective Litmus-mRFP-35S plasmids. Positions of molecular size standards, in bp, are shown on the left.

excess of Litmus-mRFP-35S plasmid encoding one of the five short RNA fragments: (i) RNA L–VII corresponding to nt 1–765 of 35S RNA and encompassing the 5′ UTR, or leader, and the first 157 nt of ORF VII; (ii) RNA VII–I (nt 766–1439) overlapping ORFs VII and I; (iii) RNA I–II nt (1440–2304) overlapping ORFs I and II; (iv) RNA II–IV (nt 2305–3000) overlapping ORFs II, III and IV and (v) 3′ UTR corresponding to the terminal nt 7928–8216 (Figure 7A). Total RNAs were then isolated from nuclear, cytoplasmic or total fractions, and 35S RNAs were quantified by real-time RT-PCR (Figure 7B, C).

While the co-expression of RNAs VII–I, I–II, II–IV or of the 3′ UTR did not significantly influence the nuclear export of 35S RNAs, that of the L–VII fragment induced a strong nuclear retention of 35S viral RNAs (Figure 7B), suggesting a possible hijacking of the export machinery by the overexpressed RNA fragment. This mainly corresponds to the 35S leader region, and was detected by RT-PCR in total RNA fractions of transfected protoplasts, as for the four other RNA fragments (Figure 7D, E). The total 35S RNAs accumulation was unaffected by the co-expression of any of the RNA fragments (Figure 7C), indicating

that transcription efficiency was not modified under these conditions.

The L–VII RNA fragment (Figure 7A) that we propose to target the nuclear export machinery, contains in 5′ a 74-nt unstructured sequence harbouring a short ORF (sORF A, nt 57–68), which is essential for ribosome shunting during translation (82). It is followed by a stable helical section of a large stem-loop secondary structure of 482 nt (83) containing five additional sORFs (for the Cabb B-JI isolate) but also the poly(A) signal and the first splicing donor (SD) site located, respectively, on the ascending and descending arms of a middle section of the stem-loop structure (84). The 35S pregenomic RNA packaging signal that interacts with the P4 coat protein is exposed on the uppermost section of the stem-loop structure (nt 288–355) (85). The 209 nt following the stem-loop and preceding ORF VII are probably unstructured and end with the $tRNA^{Meti}$ primer binding site (PBS) (nt 596–609), where the P5 RT is loaded (86).

To further investigate whether some sections of the L–VII fragment are more specifically involved in the nuclear export, we split the sequence into eight different sections (Supplementary Figure S7C, upper part): the stem–loop (SL), its left (SL_Left) and right (SL_Right) arms, the bottom (SL_Bottom) and top (SL_Top) sections, the 5′ (L_5′) and 3′ ends (L_3′) of the leader, and the single-stranded sequence preceding ORF VII (SS_3′). The respective plasmids were then co-transfected, together with pCaMV-GFP, in protoplasts, and the nuclear export of 35S RNAs was analysed as previously described (Supplementary Figure S7A). The important nuclear retention of 35S RNAs was confirmed in this assay. Moreover, to a lesser extent, a significant inhibition effect was observed only with the co-expression of the SL.

These results suggest that two elements might be recognised by the export machinery, the highly structured SL and an additional element located at sequences upstream or downstream. Disrupting the SL structure in separate arms (SL_Left with the poly(A) signal, and SL_Right with the SD site) or expressing only sections of it (SL_Bottom, SL_Top with the packaging signal, L_5′, L_3′ and SS-3′ both containing the PBS) completely abolished the competition for the export proteins, between these short RNA fragments and the 35S RNAs that were here efficiently exported into the cytoplasm (Supplementary Figure S7A). The total 35S RNA accumulation was again unchanged by the expression of these additional RNA fragments (Supplementary Figure S7B), detected in transfected protoplasts by RT-PCR (Supplementary Figure S7C, D).

To further confirm that the 5′ NTR of CaMV is involved in nuclear export, we used an unspliced reporter RNA assay (87). The reporter RNA contains the luciferase coding sequence within an inefficiently spliced intron derived from the HIV-1 *env* gene and harbours, besides the inefficient splice donor and acceptor sites, the Rev response element (RRE) (Figure 8A). In human cells, the few spliced RNAs are exported but lose the luciferase gene. The unspliced RNA still has the luciferase sequence but is actively retained in the nucleus and does not allow luciferase expression either. To adapt the reporter RNA, we placed the *env-luciferase-RRE* expression cassette under the control of the CaMV 35S promoter and the NOS terminator, and cloned within the RRE either (i) the CaMV 5′ UTR (L–VII) or (ii) a mutated variant ($L–VII_{mut}$), in which the inefficient splice donor site D4 (nt 481–482) and the cryptic Db (nt 456–457) (49) were inactivated or (iii) the 35S (I–II) fragment, or (iv) the CTE of MMPV (Figure 8A). The resulting plasmids were transfected in WT or TREX mutant Arabidopsis protoplasts and luciferase activity was measured at 20 hpt. Luciferase was expressed even with the original Luc-RRE construct (Figure 8B, white bars), at different levels in WT or TREX mutants, indicating that, unlike in human cells, the unspliced reporter RNA is exported in Arabidopsis. This result can be explained by the fact that intron retention (IR) is the most prevalent alternative splicing event in plants, with observed frequencies as high as 64% in Arabidopsis, and that IR transcripts often escape nonsense-mediated decay (NMD), and are exported into the cytoplasm (88). The addition of the WT or mutant CaMV 5′ UTR (Figure 8B) significantly increased the luciferase activity both in WT and in TREX mutant Arabidopsis. The detection of the different reporter RNAs by RT-PCR (Figure 8C) shows that both their total amounts and splicing were unaffected, since only the unspliced isoforms (>2700) were amplified. This suggests that the enhanced luciferase activity was probably due to an enhanced nuclear export of its mRNA. Conversely, in the presence of 35S RNA fragment (I–II) or the CTE, the luciferase activity was lower, indicating that the RNA export was less efficient and that the MPMV CTE is probably not functional in plants.

Our combined results demonstrate that the 5′ UTR of 35S RNA, and particularly its stable SL secondary structure, behaves as an export-enhancing element that might be recognised by the export proteins. Therefore, we investigated whether this region can effectively interact with some RNA-binding proteins of the TREX complex, such as ALY1, ALY3 (32) or MOS11 (54).

MOS11 and export adaptors ALY1 and ALY3 can interact with CaMV 35S RNA *in vitro*

It was shown that both MOS11 (54) and ALY1 (32) bind *in vitro* 25-nucleotide RNA duplexes and single-stranded RNAs. We investigated whether these proteins would also interact with the complex secondary structure of the 35S RNA leader region, which folds into a large stem interrupted by several loops, short hairpins and four side stems (83,89).

To test the putative RNA-protein interactions, we performed *in vitro* binding EMSA assays with RNA L–VII (765 nt) and I–II (865 nt), produced and radiolabelled *in vitro* (Figure 9A), and ALY1, ALY3, MOS11 or EGFP (as control), all expressed in bacteria and affinity-purified (Figure 9B and Supplementary Figure S8). Both ALY1, ALY3 and EGFP were His_6-tagged and expressed fused to the GB1 polypeptide to increase protein solubility in *E. coli* (32).

In the presence of 10 or 20 μM of the control protein His_6-GB1-EGFP, the electrophoretic mobility of neither RNA L–VII nor RNA I–II was reduced (Figure 9C), demonstrating that this protein, harbouring the same tags as ALY1 and ALY3, does not interact with any of the 35S RNA fragments. On the contrary, increasing amounts of

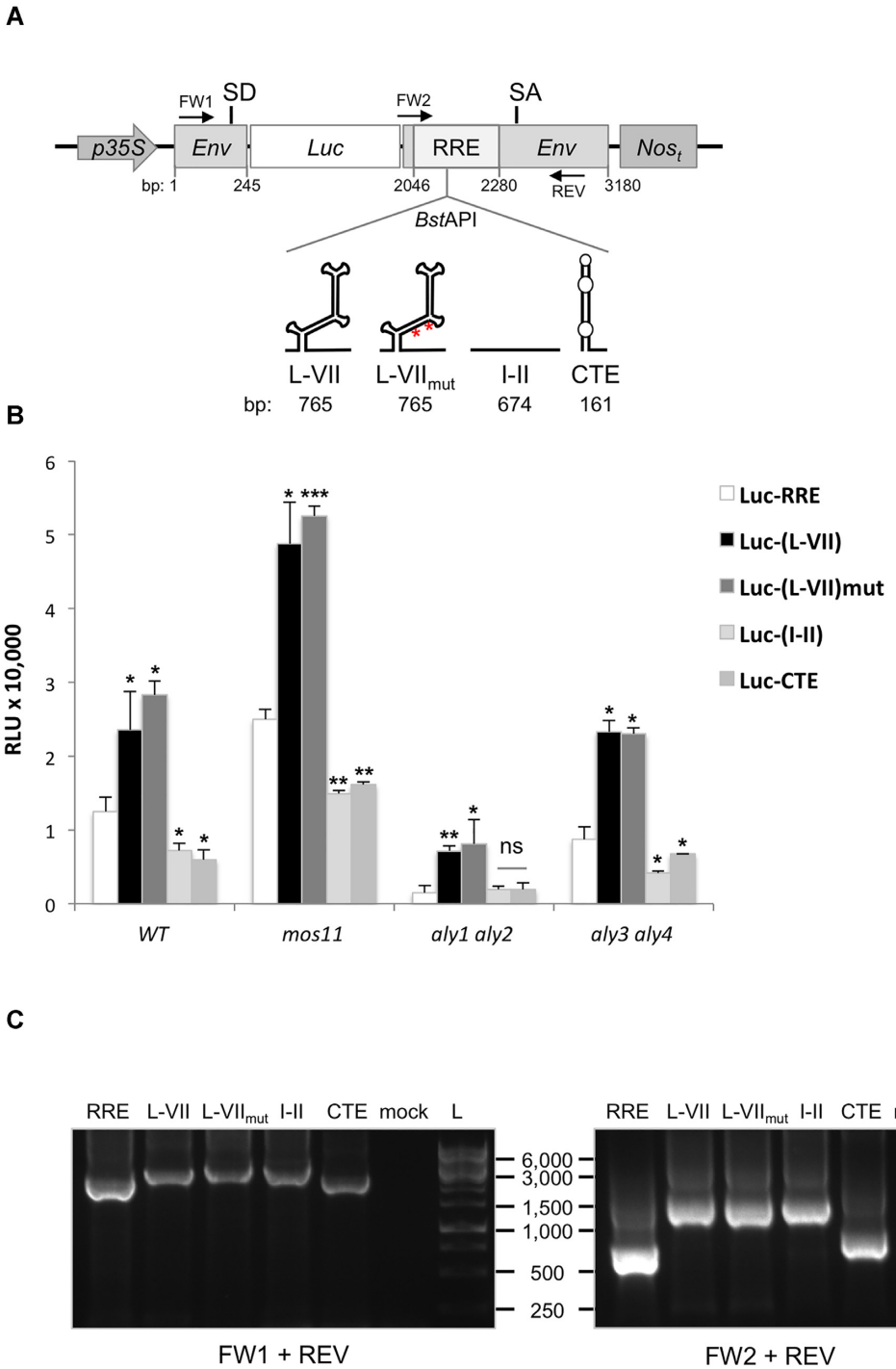

Figure 8. The 5′ UTR of CaMV 35S RNA enhances the nuclear export of a reporter luciferase mRNA. (**A**) Schematic representation of the Luc-RRE reporter and the resulting constructs obtained by cloning of 35S RNA fragments L–VII, L–VII$_{mut}$ (the two red asterisks show the positions of the two mutated splice donor sites Db and D4) and I–II, and MPMV CTE in the *Bst*API restriction site (*p35S*: 35S RNA promoter, *Env*: HIV-1 ENV coding sequence, *Luc*: firefly luciferase, RRE: REV response element, *NOS$_t$*: NOS terminator, SD: splice donor site, SA: splice acceptor site). (**B**) WT/*CA-rop2, mos11*, *aly1 aly2* and *aly3 aly4* protoplasts were transfected with the above described reporter plasmids and 20 hpt luciferase activities (RLU: relative light units) were measured in triplicate in three different experiments, normalised to the transfection efficiency by assaying for mRFP fluorescence and averaged. Significance was tested with a Student's unpaired two-sample t-test (ns, not significant, $P > 0.05$, * $P < 0.05$, ** $P < 0.01$, *** $P < 0.001$). (**C**) The reporter mRNAs expression in the transfected protoplasts was analysed by RT-PCR with specific primers, the position of which is indicated by black arrows in (**A**).

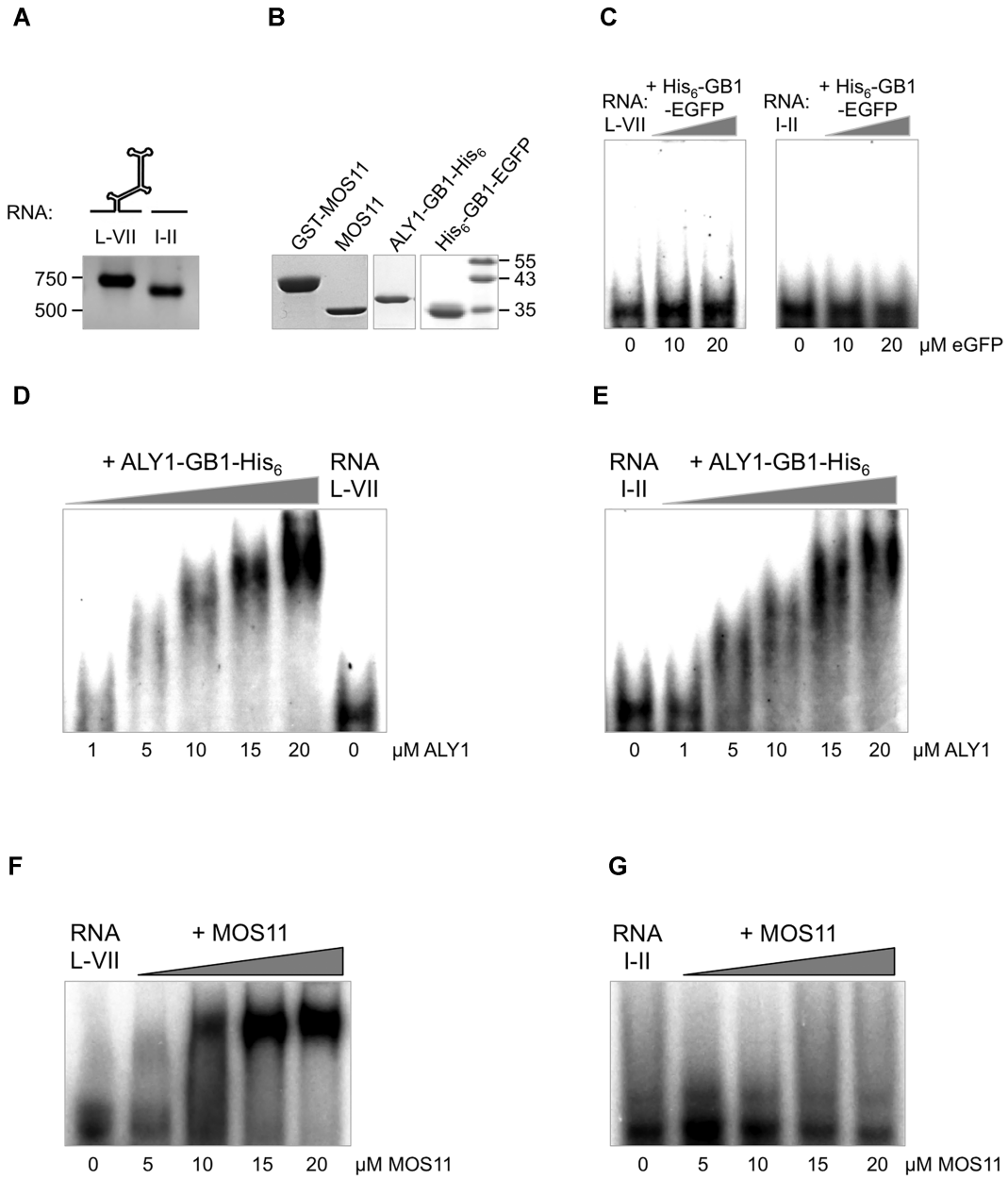

Figure 9. CaMV 35S RNA can bind ALY1 and MOS11 *in vitro*. (**A**) 35S RNA fragments L–VII and I–II were *in vitro* synthesised by T7 RNA polymerase, labelled with [α-^{32}P]-UTP, and analysed by denaturing agarose electrophoresis. (**B**) ALY1 and EGFP (as control), and MOS11 were expressed in *E. coli* as GB1-His_6 (ALY1 and EGFP) or GST (MOS11) fusion proteins, purified by affinity chromatography, and examined by SDS-PAGE. (**C**) EMSA with ≈ 5000 cpm L–VII or I–II RNA and 0, 10 or 20 μM purified His_6-GB1-EGFP, analysed by non-denaturing electrophoresis and autoradiography. EMSA with ≈ 5,000 cpm RNA L–VII (**D, F**) or I–II (**E, G**) and increasing amounts (0 to 20 μM) of purified ALY1-GB1-His_6 (D, E) or MOS11 (F, G), analysed by non-denaturing electrophoresis and autoradiography. Positions of molecular size standards in nt (A) or kDa (B) are shown on the left and right, respectively.

ALY1-GB1-His_6 (0–20 μM) progressively reduced RNA L–VII migration (Figure 9D): compared to free RNA L–VII (0 μM ALY1), the band-shift occurred in the presence of 5 μM ALY1, and its intensity increased at 10, 15 and 20 μM protein suggesting that ALY1 interacts with RNA L–VII and that multiple copies of the proteins are progressively loaded on the 765 nt long fragment. Since RNA L–VII is composed of 5′ and 3′ unstructured sequences (74 and 209 nt, respectively), and the 482 nt SL, it is probable that ALY1 interacts with both structured and unstructured RNA sections, forming increasingly larger ribonucleoproteins, the migration of which is progressively shifted. This observation is consistent with the results of Pfaff *et al.* (32) who demonstrated that Arabidopsis ALY1 behaves as a typical RNA-binding protein that interacts via its central RNA recognition motif (RRM) with both single-stranded (ss) and double-stranded (ds) RNA, and even with ssDNA. However, it exhibits a preference for ssRNA. The RRM alone binds weakly, and binding is strongly enhanced by the termini, particularly the N-terminus (32).

Consistent with these findings, it is unsurprising that we observed almost the same gel-shift of RNA I–II in the presence of increasing amounts (0 to 20 μM) of ALY1 (Figure 9E), starting, as for L-VII, at 5 μM protein. Although unnecessary for 35S RNA nuclear export, this RNA interacted with export adaptors ALY1, as did the *cis*-acting fragment L–VII.

We also tested ALY3 for its ability to interact with 35S RNA, since Pfaff *et al.* (32) had shown that ALY1 and ALY2 (54% amino acid sequence identity) as well as ALY3 and ALY4 (70% amino acid sequence identity) share a high degree of sequence similarity, whereas the similarity of ALY1/2 versus ALY3/4 is clearly lower (less than 42% amino acid sequence identity). Moreover, ALY3 and ALY4 are strongly enriched in nucleoli, whereas ALY1 and ALY2 are clearly less prominent in nucleoli relative to the nucleoplasm. As shown in Supplementary Figure S8, ALY3 also binds to both the L–VII and I–II RNA fragments but with less affinity, since the single band-shifts only occurred with 15 and 20 μM ALY3 for the L–VII RNA and with 20 μM ALY3 for the RNA I–II.

We observed the same RNA-binding properties of ALY1 and ALY3 towards a CaMV-unrelated but also highly structured RNA, the HIV-1 RRE element (87) (data not shown). Together, these results demonstrate that the ALY adaptor proteins can interact with complex secondary structures.

MOS11 RNA-binding was markedly different. As shown (Figure 9F), MOS11 associated with the 35S L–VII RNA fragment in a concentration-dependent manner. However, contrary to ALY1, RNA migration was not further decelerated while increasing the protein concentration (10 to 20 μM). This observation suggests that MOS11 cannot interact randomly, as does ALY1, with several binding sites on the 765 nt long L–VII RNA.

Moreover, MOS11 did not associate with the I–II RNA fragment (Figure 9G), which, according to mfold (90), is presumably lacking a stable secondary structure. These findings can be correlated with previous work, which showed that this RNA-binding protein associates better with dsRNA than with ssRNA (54), further suggesting that MOS11 preferentially interacts with the 482 nt SL of the 35S RNA leader region.

DISCUSSION

Host cellular machineries play indispensable roles in virus life cycles. Among them is the nuclear export machinery that allows mRNAs to reach the cytoplasm to be translated. The export receptor TAP, which is conserved in yeast and metazoans (91), does not exist in Arabidopsis, despite the TREX adaptor complex being conserved in plants. The main role of this TREX complex is to recognise and interact with cargo mRNAs before recruiting the exportin proteins.

In this study, we described for the first time the mechanisms used by a plant virus, CaMV, to export its 35S mRNAs out of the nucleus. We demonstrated that this export is mediated by the TREX complex and involves the THO subunit and splicing factor TEX1 (54), together with MOS11 (35,54) and the ALY adaptor proteins (32). In mutant protoplasts, deficient for the expression of one or more of the export factors, 35S RNAs were retained in the nucleus. This export inhibition explains the partial resistance of the respective Arabidopsis mutants to CaMV infection.

It has been shown that, among the six THO components (HPR1, THO2, TEX1, THO5–7), TEX1 and HPR1 are required for efficient cellular mRNA export in Arabidopsis (54,92,93). However, in our experiments, CaMV 35S RNA nuclear export was unaffected in the single mutant *tex1*, as well as in *hpr1* or *tho6* protoplasts, and the respective mutant plants displayed the same susceptibility to CaMV (data not shown). These results suggest that the particular composition and assembly of the THO core are probably less important for the export of viral mRNAs than of cellular mRNAs and that differences exist in the TREX-dependent export of these different mRNA populations.

The export adaptor MOS11 proved essential for 35S RNA export, because nuclear export was reduced by almost 50% in the absence of this protein. This observation is consistent with the strong nuclear retention of cellular mRNAs described for *mos11* plants (54), and, like for cellular mRNAs, the export inhibition of 35S RNA increased in the double mutant *mos11 tex1*. One can imagine that TEX1 enhances the effect of MOS11 and is important for CaMV because of its role in splicing: TEX1 interacts with several splicing factors and co-localises in a speckled pattern in the nucleoplasm with SR proteins, and its absence in *tex1* and *tex1 mos11* mutants is responsible for quantitative changes in alternatively spliced transcript variants (54). According to these findings, it cannot be excluded that in the absence of TEX1, CaMV 35S splicing is modified leading to the accumulation of viral RNA isoforms that are better retained in nuclei of *tex1 mos11* protoplasts. However, when examining by RT-PCR the splicing profile of 35S RNA in *tex1* single and double mutants, we did not detect significant differences: the four spliced and the unspliced isoform were present at levels comparable to those in WT protoplasts (data not shown). This suggests that the potentiating effect of TEX1 on export is not linked to splicing and the mechanism thus requires further clarification.

The most important proteins for CaMV 35S RNA nuclear export are ALY1–4, since the export was strongly inhibited in *aly1 aly2* and *aly3 aly4* double mutants, and especially in the *4xaly* quadruple mutant, where this inhibition exceeded 90%. Consistent with this observation, 75% of *4xaly* plants displayed resistance to CaMV infection.

All ALYs are ubiquitously expressed in vegetative tissues but display different subnuclear localisations. ALY3 and ALY4 are present at higher levels in nucleoli than ALY1 and ALY2 (32). Considering the disruption in viral mRNA export in both ALY double mutants, it is surprising that these plants did not show more resistance to CaMV. Our results suggest that there must be a functional compensation *in planta* for the lack of ALYs by the two other ALY paralogues in each case. It is also surprising that, despite the strong indisputable role of ALYs in viral and cellular mRNA export, *4xaly* plants are severely affected but still viable and not completely resistant to CaMV infection. Conversely, yeast cells lacking Yra1, the orthologue of ALY, are not viable (94,95). These findings can be explained with the recently demonstrated existence, in Arabidopsis, of two additional ALY functional homologues, the UAP56 interacting export factors UIEF1 and 2, which can also bind RNA

(33). The *2xuief* double mutant displays only modest growth defects and is mildly affected in nuclear mRNA accumulation. However, the sextuple *4xaly 2xuief* mutation, without markedly exacerbating *4xaly* growth and reproductive defects, significantly enhances the nuclear mRNA accumulation compared to *4xaly* plants (33). It would therefore be of interest to investigate 35S RNA nuclear export in this newly generated mutant, as well as its susceptibility to CaMV infection. We would expect an almost complete inhibition of both, considering the results we obtained in *4xaly* plants. Another possibility may be the involvement of shuttling SR proteins that act as adaptors in other organisms (24).

The involvement of the TREX complex in the nuclear export of viral mRNAs is unsurprising, since TREX is part of the major export pathway of TAP/p15 transporters that are hijacked by many viruses in mammals, such as simple and complex retroviruses (96–101) and DNA viruses such as adenoviruses (102,103), herpesviruses (41,104,105) and HBV (106–108). Among these viruses, many use a specific and generally multifunctional viral protein that interacts both with viral mRNAs and with one or several export factors and thus recruits the export machinery. Herpesviruses ICP27/ORF57 proteins, for example, can associate with the TAP transporter (109), ALY (40), UIF (42) and CIP29 (43).

Therefore, it was interesting to find that for CaMV, at least one viral protein, PR/RT P5, is important for viral mRNA export, as demonstrated in protoplasts transfected with a mutated pCaMV-GFP, in which all viral proteins or (at least) P5 cannot be produced. In these protoplasts the 35S RNAs were massively sequestrated in the nucleus. This export deficiency was efficiently rescued *in trans* by full-length P5 but not by its individual functional PR or RTRH domains.

To our knowledge, the involvement of RTs in the nuclear export of viral mRNAs has not been described for retroviruses or pararetrovirus HBV. However, the involvement of viral RNA-dependent RNA polymerases was demonstrated for influenza A virus (IAV), the heterotrimeric polymerase of which recruits cellular helicase DDX19 (also known as DBP5) on viral mRNPs to enhance their nuclear export (110). It was also recently shown that the same polymerase, especially its PB1 and PB2 subunits, recruit cellular RNA helicase eIF4A3, which is part of the EJC, to promote viral mRNA splicing and nuclear export of the spliced mRNAs (111).

The role of P5 in nuclear export can be easily understood when considering several previous findings. As genome encapsidation probably occurs during reverse transcription of 35S unspliced (pregenomic) RNA (112,113), at least three copies P5 must be present inside the virions (114), which are required to perform the negative-strand synthesis and the discontinuous synthesis of the positive-strand DNA (86,115). After capsid dissociation on nuclear pores, some capsid and P5 proteins are probably imported into the nucleus in association with the viral genome. Pfeiffer *et al.* (75) also described an increase in a DNA polymerase of ca. 75 kDa, present in infected turnip nuclear extracts. During the viral life cycle, P5 together with P6, which is independently expressed from its 19S RNA, and P1 synthesised from unspliced 35S RNAs, accumulate early in turnip protoplasts (116). This observation is surprising considering that the main functions of P5 (genome replication and capsid maturation) occur late in the viral cycle, and suggests other potentially early role(s) for P5. Therefore, we investigated whether P5, important for viral mRNA export, can interact with export factors. We demonstrated by GST pull-down assays, that P5, and especially its central RT domain, associates with MOS11 *in vitro*.

In the same GST pull-down experiments, we found that a second viral protein, P4, probably unprocessed and as a dimer, interacts with MOS11 *in vitro*. This interaction suggests that P4 is also involved in TREX-mediated viral mRNA export. The simultaneous absence of P5 and P4 in protoplasts transfected with pCaMV-GFP-P6_STOP could explain the strong nuclear retention of 35S RNA. In mammals, the HBV core protein involvement in the nuclear export of some viral mRNAs by direct loading, not of CIP29 but of transporter TAP/p15, was described (117).

CaMV coat proteins that are proteolytically matured (by P5 and unidentified cellular proteinases) to remove N- and C-termini, can enter the nucleus via their Nt NLS, which becomes accessible only on cleavage (46). However, using EGFP fusion proteins, we observed that not only full-length P4 protein but also uncleaved P5, in which we discovered two functional bipartite NLSs, displays a nucleocytoplasmic distribution, with typical cytoplasmic aggregates coherent with the cytoplasmic functions of both proteins. Additionally, they perfectly co-localised with MOS11-mRFP in the nucleus. This nuclear co-localisation and the related co-immunoprecipitation assays suggests that the physical interaction observed *in vitro* between the two viral proteins and the export factor occurs in the nucleus and promotes the nuclear export of viral mRNAs.

We finally investigated the presence of potential *cis*-acting elements in the 35S RNAs that are important for the loading of the export machinery. We demonstrated by competition experiments and reporter RNA assays in protoplasts that an RNA fragment corresponding to the 5′ leader region followed by the first third of ORF VII (L–VII) efficiently outcompetes full-length viral RNAs for export factors and enhances the nuclear export of a reporter RNA. The overexpression of the highly structured SL of the leader (83), which harbours several important elements, such as five regulatory sORFs, the conditional poly(A) site, the coat protein P4 binding site and the first splice donor site D4, and which is bypassed during translation by ribosome shunting (82), also inhibited viral RNA nuclear export but to a lesser extent. This observation suggests that the short 5′ and/or the longer 3′ regions that flank the SL are important for export. Consistent with our previous results on the role of P5, we can expect that this additional *cis*-acting element is the $tRNA^{Meti}$ PBS, which precedes ORFVII and where P5 is loaded on 35S RNA (86).

Finally, we showed that the RNA-binding adaptors ALY1 and ALY3 (32) can interact, probably without specificity, with the 35S RNA 5′ leader (L–VII) and/or with a downstream coding sequence (I-II) unrelated to export. Most important, however, was the observation that MOS11 preferentially interacts with the structured 35S RNA leader but not with the I–II control RNA, consistent with previous work showing that this RNA-binding protein associates better with dsRNA than with ssRNA (54). One can imag-

ine that the TREX complex can be further preferentially enriched on the 35S 5′ secondary structure by the interactions existing between MOS11, P4 loaded on its binding site on the top of the SL, and/or P5 recruited to the downstream located PBS, in the presence or absence of $tRNA^{Meti}$ primer.

Based on the results presented in this study, we can predict the following model for CaMV 35S mRNA nuclear export. When the viral DNA is released from the virion into the nucleoplasm, host DNA repair enzymes repair the gaps left by RT during the previous replication cycle to create covalently closed molecules. This closed viral DNA is then transcribed by Pol II into pregenomic polycistronic 35S RNA, 70% of which is alternatively spliced, and into subgenomic 19S RNA, which is the mRNA for the viral protein P6. The unspliced 35S RNA and three out of the four spliced isoforms contain the highly structured 5′ leader, whereas the last isoform and 19S RNA do not. During the first round of viral transcription only a few copies of coat protein P4 and RT P5 are present in the nucleus. Thus, a first minimal round of nuclear export might occur, during which TREX complexes might be loaded on viral mRNAs mainly by CBCs and EJCs, probably more efficiently on the leader-containing mRNA species than for the others, which can be considered as regular cellular mRNAs. In the cytoplasm, these mRNAs are then translated, and viral proteins progressively accumulate. P5 polyprotein and P4 coat precursor enter the nuclei via their NLSs. There, they bind their respective recognition sites on the leader-containing 35S RNAs and, interacting with MOS11, might promote the recruitment of TREX and enhance the nuclear export of these viral RNAs.

DATA AVAILABILITY

All datasets generated for this study are included in the manuscript and/or the Supplementary Files.

SUPPLEMENTARY DATA

Supplementary Data are available at NAR Online.

ACKNOWLEDGEMENTS

We gratefully acknowledge Martin Drucker (INRAE, Colmar, France) for kindly providing pCaMV-GFP, Zhenbiao Yang (UC, Riverside, US) for *CA-rop2* seeds, Manfred Heinlein and Nicolas Pitzalis (IBMP, Strasbourg, France) for TuMV, Jean-Christophe Paillart (IBMC, Strasbourg, France) for pNL4.3, Daniel Clesse (protein production and purification facility, IBMP) for help with ALY1 purification, Abdelmalek Alioua and Sandrine Koechler (gene expression analysis facility, IBMP) for sequencing and qPCR set up, Michel Kernéis (plant production facility, IBMP) for precious help with Arabidopsis production, Philippe Hammann, Johana Chicher and Lauriane Kuhn (proteomics facility Strasbourg-Esplanade) for set up and analysis of mass spectrometry experiments, Anita Kaltak (Université de Strasbourg) for excellent technical assistance, Corinne Keichinger (INRAE, Colmar, France), Khalid Amari (JKI, Braunschweig, Germany) and Esther Lechner (IBMP, Strasbourg, France), for providing plasmids, Stéphane Blanc (INRAE, Montpellier, France), Anne-Marie Duchêne and David Gilmer (IBMP, Strasbourg, France) for providing antibodies, Quentin Chevalier and Vianney Poignavent (IBMP, Strasbourg, France) for kindly preparing and providing the anti-EGFP magnetic beads, and Marie Meister (Musée de Zoologie, Strasbourg, France) and Todd Blevins (IBMP) for critical reading of the manuscript. The graphical abstarct was created with Biorender.com.

FUNDING

Centre National de la Recherche Scientifique and Université de Strasbourg; Julie Kubina, Clément Bouton and Jón Pol Gales PhD were/are supported by fellowships from Ministère de l'Enseignement Supérieur, de la Recherche et de l'Innovation and from Université de Strasbourg (to J.K.); the mRNA export project in the Grasser laboratory is financially supported by the German Research Foundation (DFG) [SFB960 to K.D.G.]. Funding for open access charge: Institut de Biologie Moléculaire des Plantes.
Conflict of interest statement. None declared.

REFERENCES

1. Ramanathan,A., Robb,G.B. and Chan,S.-H. (2016) mRNA capping: biological functions and applications. *Nucleic Acids Res.*, **44**, 7511–7526.
2. Girard,C., Will,C.L., Peng,J., Makarov,E.M., Kastner,B., Lemm,I., Urlaub,H., Hartmuth,K. and Lührmann,R. (2012) Post-transcriptional spliceosomes are retained in nuclear speckles until splicing completion. *Nat. Commun.*, **3**, 994.
3. Stewart,M. (2019) Polyadenylation and nuclear export of mRNAs. *J. Biol. Chem.*, **294**, 2977–2987.
4. Delaleau,M. and Borden,K.L.B. (2015) Multiple export mechanisms for mRNAs. *Cells*, **4**, 452–473.
5. Heath,C.G., Viphakone,N. and Wilson,S.A. (2016) The role of TREX in gene expression and disease. *Biochem. J.*, **473**, 2911–2935.
6. Williams,T., Ngo,L.H. and Wickramasinghe,V.O. (2018) Nuclear export of RNA: different sizes, shapes and functions. *Semin. Cell Dev. Biol.*, **75**, 70–77.
7. Kang,Y., Bogerd,H.P., Yang,J. and Cullen,B.R. (1999) Analysis of the RNA binding specificity of the human tap protein, a constitutive transport element-specific nuclear RNA export factor. *Virology*, **262**, 200–209.
8. Teplova,M., Wohlbold,L., Khin,N.W., Izaurralde,E. and Patel,D.J. (2011) Structure-function studies of nucleocytoplasmic transport of retroviral genomic RNA by mRNA export factor TAP. *Nat. Struct. Mol. Biol.*, **18**, 990–998.
9. Björk,P. and Wieslander,L. (2017) Integration of mRNP formation and export. *Cell. Mol. Life Sci.*, **74**, 2875–2897.
10. Masuda,S., Das,R., Cheng,H., Hurt,E., Dorman,N. and Reed,R. (2005) Recruitment of the human TREX complex to mRNA during splicing. *Genes Dev.*, **19**, 1512–1517.
11. Hautbergue,G.M., Hung,M.-L., Golovanov,A.P., Lian,L.-Y. and Wilson,S.A. (2008) Mutually exclusive interactions drive handover of mRNA from export adaptors to TAP. *Proc. Natl. Acad. Sci. U.S.A.*, **105**, 5154–5159.
12. Hautbergue,G.M., Hung,M.-L., Walsh,M.J., Snijders,A.P.L., Chang,C.-T., Jones,R., Ponting,C.P., Dickman,M.J. and Wilson,S.A. (2009) UIF, a New mRNA export adaptor that works together with REF/ALY, requires FACT for recruitment to mRNA. *Curr. Biol.*, **19**, 1918–1924.
13. Shen,J., Zhang,L. and Zhao,R. (2007) Biochemical characterization of the ATPase and helicase activity of UAP56, an essential pre-mRNA splicing and mRNA export factor. *J. Biol. Chem.*, **282**, 22544–22550.
14. Fukuda,S., Wu,D.W., Stark,K. and Pelus,L.M. (2002) Cloning and characterization of a proliferation-associated cytokine-inducible protein, CIP29. *Biochem. Biophys. Res. Commun.*, **292**, 593–600.

15. Cheng,H., Dufu,K., Lee,C.-S., Hsu,J.L., Dias,A. and Reed,R. (2006) Human mRNA export machinery recruited to the 5′ end of mRNA. *Cell*, **127**, 1389–1400.
16. Chi,B., Wang,Q., Wu,G., Tan,M., Wang,L., Shi,M., Chang,X. and Cheng,H. (2013) Aly and THO are required for assembly of the human TREX complex and association of TREX components with the spliced mRNA. *Nucleic Acids Res.*, **41**, 1294–1306.
17. Viphakone,N., Sudbery,I., Griffith,L., Heath,C.G., Sims,D. and Wilson,S.A. (2019) Co-transcriptional loading of RNA export factors shapes the human transcriptome. *Mol. Cell*, **75**, 310–323.
18. Le Hir,H., Gatfield,D., Izaurralde,E. and Moore,M.J. (2001) The exon-exon junction complex provides a binding platform for factors involved in mRNA export and nonsense-mediated mRNA decay. *EMBO J.*, **20**, 4987–4997.
19. Dufu,K., Livingstone,M.J., Seebacher,J., Gygi,S.P., Wilson,S.A. and Reed,R. (2010) ATP is required for interactions between UAP56 and two conserved mRNA export proteins, Aly and CIP29, to assemble the TREX complex. *Genes Dev.*, **24**, 2043–2053.
20. Viphakone,N., Hautbergue,G.M., Walsh,M., Chang,C.-T., Holland,A., Folco,E.G., Reed,R. and Wilson,S.A. (2012) TREX exposes the RNA-binding domain of Nxf1 to enable mRNA export. *Nat. Commun.*, **3**, 1006.
21. Wickramasinghe,V.O. and Laskey,R.A. (2015) Control of mammalian gene expression by selective mRNA export. *Nat. Rev. Mol. Cell Biol.*, **16**, 431–442.
22. Kiesler,E., Miralles,F. and Visa,N. (2002) HEL/UAP56 binds cotranscriptionally to the Balbiani ring pre-mRNA in an intron-independent manner and accompanies the BR mRNP to the nuclear pore. *Curr. Biol.*, **12**, 859–862.
23. Nojima,T., Hirose,T., Kimura,H. and Hagiwara,M. (2007) The interaction between Cap-binding complex and RNA export factor is required for intronless mRNA export. *J. Biol. Chem.*, **282**, 15645–15651.
24. Huang,Y. and Steitz,J.A. (2001) Splicing factors SRp20 and 9G8 promote the nucleocytoplasmic export of mRNA. *Mol. Cell*, **7**, 899–905.
25. Hargous,Y., Hautbergue,G.M., Tintaru,A.M., Skrisovska,L., Golovanov,A.P., Stevenin,J., Lian,L.-Y., Wilson,S.A. and Allain,F.H.-T. (2006) Molecular basis of RNA recognition and TAP binding by the SR proteins SRp20 and 9G8. *EMBO J.*, **25**, 5126–5137.
26. Tintaru,A.M., Hautbergue,G.M., Hounslow,A.M., Hung,M.-L., Lian,L.-Y., Craven,C.J. and Wilson,S.A. (2007) Structural and functional analysis of RNA and TAP binding to SF2/ASF. *EMBO Rep.*, **8**, 756–762.
27. Lei,H., Dias,A.P. and Reed,R. (2011) Export and stability of naturally intronless mRNAs require specific coding region sequences and the TREX mRNA export complex. *Proc. Natl. Acad. Sci. U.S.A.*, **108**, 17985–17990.
28. Lei,H., Zhai,B., Yin,S., Gygi,S. and Reed,R. (2013) Evidence that a consensus element found in naturally intronless mRNAs promotes mRNA export. *Nucleic Acids Res.*, **41**, 2517–2525.
29. Ehrnsberger,H.F., Grasser,M. and Grasser,K.D. (2019) Nucleocytosolic mRNA transport in plants: export factors and their influence on growth and development. *J. Exp. Bot.*, **70**, 3757–3763.
30. Yelina,N.E., Smith,L.M., Jones,A.M.E., Patel,K., Kelly,K.A. and Baulcombe,D.C. (2010) Putative Arabidopsis THO/TREX mRNA export complex is involved in transgene and endogenous siRNA biosynthesis. *Proc. Natl. Acad. Sci. U.S.A.*, **107**, 13948–13953.
31. Uhrig,J.F., Canto,T., Marshall,D. and MacFarlane,S.A. (2004) Relocalization of nuclear ALY proteins to the cytoplasm by the tomato bushy stunt virus P19 pathogenicity protein. *Plant Physiol.*, **135**, 2411–2423.
32. Pfaff,C., Ehrnsberger,H.F., Flores-Tornero,M., Sørensen,B.B., Schubert,T., Längst,G., Griesenbeck,J., Sprunck,S., Grasser,M. and Grasser,K.D. (2018) ALY RNA-Binding proteins are required for Nucleocytosolic mRNA transport and modulate plant growth and development1[OPEN]. *Plant Physiol.*, **177**, 226–240.
33. Ehrnsberger,H.F., Pfaff,C., Hachani,I., Flores-Tornero,M., Sørensen,B.B., Längst,G., Sprunck,S., Grasser,M. and Grasser,K.D. (2019) The UAP56-Interacting export factors UIEF1 and UIEF2 function in mRNA export. *Plant Physiol.*, **179**, 1525–1536.
34. Kammel,C., Thomaier,M., Sørensen,B.B., Schubert,T., Längst,G., Grasser,M. and Grasser,K.D. (2013) Arabidopsis DEAD-box RNA helicase UAP56 interacts with both RNA and DNA as well as with mRNA export factors. *PLoS One*, **8**, e60644.
35. Germain,H., Qu,N., Cheng,Y.T., Lee,E., Huang,Y., Dong,O.X., Gannon,P., Huang,S., Ding,P., Li,Y. *et al.* (2010) MOS11: a new component in the mRNA export pathway. *PLoS Genet.*, **6**, e1001250.
36. Gales,J.P., Kubina,J., Geldreich,A. and Dimitrova,M. (2020) Strength in diversity: nuclear export of viral RNAs. *Viruses*, **12**, 1014.
37. Koffa,M.D., Clements,J.B., Izaurralde,E., Wadd,S., Wilson,S.A., Mattaj,I.W. and Kuersten,S. (2001) Herpes simplex virus ICP27 protein provides viral mRNAs with access to the cellular mRNA export pathway. *EMBO J.*, **20**, 5769–5778.
38. Malik,P., Blackbourn,D.J. and Clements,J.B. (2004) The evolutionarily conserved Kaposi's sarcoma-associated herpesvirus ORF57 protein interacts with REF protein and acts as an RNA export factor. *J. Biol. Chem.*, **279**, 33001–33011.
39. Boyne,J.R., Colgan,K.J. and Whitehouse,A. (2008) Herpesvirus saimiri ORF57: a post-transcriptional regulatory protein. *Front. Biosci. J. Virtual Libr.*, **13**, 2928–2938.
40. Tunnicliffe,R.B., Hautbergue,G.M., Kalra,P., Jackson,B.R., Whitehouse,A., Wilson,S.A. and Golovanov,A.P. (2011) Structural basis for the recognition of cellular mRNA export factor REF by herpes viral proteins HSV-1 ICP27 and HVS ORF57. *PLoS Pathog.*, **7**, e1001244.
41. Tunnicliffe,R.B., Tian,X., Storer,J., Sandri-Goldin,R.M. and Golovanov,A.P. (2018) Overlapping motifs on the herpes viral proteins ICP27 and ORF57 mediate interactions with the mRNA export adaptors ALYREF and UIF. *Sci. Rep.*, **8**, 15005.
42. Jackson,B.R., Boyne,J.R., Noerenberg,M., Taylor,A., Hautbergue,G.M., Walsh,M.J., Wheat,R., Blackbourn,D.J., Wilson,S.A. and Whitehouse,A. (2011) An interaction between KSHV ORF57 and UIF provides mRNA-adaptor redundancy in herpesvirus intronless mRNA export. *PLoS Pathog.*, **7**, e1002138.
43. Schumann,S., Baquero-Perez,B. and Whitehouse,A. (2016) Interactions between KSHV ORF57 and the novel human TREX proteins, CHTOP and CIP29. *J. Gen. Virol.*, **97**, 1904–1910.
44. Grüter,P., Tabernero,C., von Kobbe,C., Schmitt,C., Saavedra,C., Bachi,A., Wilm,M., Felber,B.K. and Izaurralde,E. (1998) TAP, the human homolog of Mex67p, mediates CTE-dependent RNA export from the nucleus. *Mol. Cell*, **1**, 649–659.
45. Chi,B., Wang,K., Du,Y., Gui,B., Chang,X., Wang,L., Fan,J., Chen,S., Wu,X., Li,G. *et al.* (2014) A sub-element in PRE enhances nuclear export of intronless mRNAs by recruiting the TREX complex via ZC3H18. *Nucleic Acids Res.*, **42**, 7305–7318.
46. Karsies,A., Merkle,T., Szurek,B., Bonas,U., Hohn,T. and Leclerc,D. (2002) Regulated nuclear targeting of cauliflower mosaic virus. *J. Gen. Virol.*, **83**, 1783–1790.
47. Haas,M., Geldreich,A., Bureau,M., Dupuis,L., Leh,V., Vetter,G., Kobayashi,K., Hohn,T., Ryabova,L., Yot,P. *et al.* (2005) The open reading frame VI product of Cauliflower mosaic virus is a nucleocytoplasmic protein: its N terminus mediates its nuclear export and formation of electron-dense viroplasms. *Plant Cell*, **17**, 927–943.
48. Kiss-László,Z., Blanc,S. and Hohn,T. (1995) Splicing of cauliflower mosaic virus 35S RNA is essential for viral infectivity. *EMBO J.*, **14**, 3552–3562.
49. Bouton,C., Geldreich,A., Ramel,L., Ryabova,L.A., Dimitrova,M. and Keller,M. (2015) Cauliflower mosaic virus transcriptome reveals a complex alternative splicing pattern. *PLoS One*, **10**, e0132665.
50. Torruella,M., Gordon,K. and Hohn,T. (1989) Cauliflower mosaic virus produces an aspartic proteinase to cleave its polyproteins. *EMBO J.*, **8**, 2819–2825.
51. Ryabova,L., Park,H.-S. and Hohn,T. (2004) Control of translation reinitiation on the cauliflower mosaic virus (CaMV) polycistronic RNA. *Biochem. Soc. Trans.*, **32**, 592–596.
52. Murashige,T. and Skoog,F. (1962) A revised medium for rapid growth and bio assays with tobacco tissue cultures. *Physiol. Plant.*, **15**, 473–497.
53. Li,H., Shen,J.J., Zheng,Z.L., Lin,Y. and Yang,Z. (2001) The Rop GTPase switch controls multiple developmental processes in Arabidopsis. *Plant Physiol.*, **126**, 670–684.
54. Sørensen,B.B., Ehrnsberger,H.F., Esposito,S., Pfab,A., Bruckmann,A., Hauptmann,J., Meister,G., Merkl,R., Schubert,T.,

Längst,G. *et al.* (2017) The Arabidopsis THO/TREX component TEX1 functionally interacts with MOS11 and modulates mRNA export and alternative splicing events. *Plant Mol. Biol.*, **93**, 283–298.
55. Lellis,A.D., Kasschau,K.D., Whitham,S.A. and Carrington,J.C. (2002) Loss-of-susceptibility mutants of Arabidopsis thaliana reveal an essential role for eIF(iso)4E during potyvirus infection. *Curr. Biol.*, **12**, 1046–1051.
56. Yoo,S.-D., Cho,Y.-H. and Sheen,J. (2007) *Arabidopsis* mesophyll protoplasts: a versatile cell system for transient gene expression analysis. *Nat. Protoc.*, **2**, 1565–1572.
57. Dimitrova,M., Imbert,I., Kieny,M.P. and Schuster,C. (2003) Protein-protein interactions between hepatitis C virus nonstructural proteins. *J. Virol.*, **77**, 5401–5414.
58. Kim,G.-D., Cho,Y.-H. and Yoo,S.-D. (2017) Regulatory functions of cellular energy sensor SNF1-Related Kinase1 for leaf senescence delay through ETHYLENE- INSENSITIVE3 Repression. *Sci. Rep.*, **7**, 3193.
59. Link,D., Schmidlin,L., Schirmer,A., Klein,E., Erhardt,M., Geldreich,A., Lemaire,O. and Gilmer,D. (2005) Functional characterization of the Beet necrotic yellow vein virus RNA-5-encoded p26 protein: evidence for structural pathogenicity determinants. *J. Gen. Virol.*, **86**, 2115–2125.
60. Khelifa,M., Massé,D., Blanc,S. and Drucker,M. (2010) Evaluation of the minimal replication time of Cauliflower mosaic virus in different hosts. *Virology*, **396**, 238–245.
61. Sorek,N., Gutman,O., Bar,E., Abu-Abied,M., Feng,X., Running,M.P., Lewinsohn,E., Ori,N., Sadot,E., Henis,Y.I. *et al.* (2011) Differential effects of prenylation and s-acylation on type I and II ROPS membrane interaction and function. *Plant Physiol.*, **155**, 706–720.
62. Revers,F. and García,J.A. (2015) Molecular biology of potyviruses. *Adv. Virus Res.*, **92**, 101–199.
63. Schepetilnikov,M., Kobayashi,K., Geldreich,A., Caranta,C., Robaglia,C., Keller,M. and Ryabova,L.A. (2011) Viral factor TAV recruits TOR/S6K1 signalling to activate reinitiation after long ORF translation. *EMBO J.*, **30**, 1343–1356.
64. Thiébeauld,O., Schepetilnikov,M., Park,H.-S., Geldreich,A., Kobayashi,K., Keller,M., Hohn,T. and Ryabova,L.A. (2009) A new plant protein interacts with eIF3 and 60S to enhance virus-activated translation re-initiation. *EMBO J.*, **28**, 3171–3184.
65. Angel,C.A., Lutz,L., Yang,X., Rodriguez,A., Adair,A., Zhang,Y., Leisner,S.M., Nelson,R.S. and Schoelz,J.E. (2013) The P6 protein of cauliflower mosaic virus interacts with CHUP1, a plant protein which moves chloroplasts on actin microfilaments. *Virology*, **443**, 363–374.
66. Amari,K., Boutant,E., Hofmann,C., Schmitt-Keichinger,C., Fernandez-Calvino,L., Didier,P., Lerich,A., Mutterer,J., Thomas,C.L., Heinlein,M. *et al.* (2010) A family of plasmodesmal proteins with receptor-like properties for plant viral movement proteins. *PLoS Pathog.*, **6**, e1001119.
67. Bonneville,J.M., Sanfaçon,H., Fütterer,J. and Hohn,T. (1989) Posttranscriptional trans-activation in cauliflower mosaic virus. *Cell*, **59**, 1135–1143.
68. Gowda,S., Wu,F.C., Scholthof,H.B. and Shepherd,R.J. (1989) Gene VI of figwort mosaic virus (caulimovirus group) functions in posttranscriptional expression of genes on the full-length RNA transcript. *Proc. Natl. Acad. Sci. U.S.A.*, **86**, 9203–9207.
69. Fütterer,J., Gordon,K., Sanfaçon,H., Bonneville,J.M. and Hohn,T. (1990) Positive and negative control of translation by the leader sequence of cauliflower mosaic virus pregenomic 35S RNA. *EMBO J.*, **9**, 1697–1707.
70. Scholthof,H.B., Gowda,S., Wu,F.C. and Shepherd,R.J. (1992) The full-length transcript of a caulimovirus is a polycistronic mRNA whose genes are trans activated by the product of gene VI. *J. Virol.*, **66**, 3131–3139.
71. Takatsuji,H., Yamauchi,H., Watanabe,S., Kato,H. and Ikeda,J.E. (1992) Cauliflower mosaic virus reverse transcriptase. Activation by proteolytic processing and functional alteration by terminal deletion. *J. Biol. Chem.*, **267**, 11579–11585.
72. Ani,R.A., Pfeiffer,P., Lebeurier,G. and Hirth,L. (1979) The structure of cauliflower mosaic virus I. pH-Induced structural changes. *Virology*, **93**, 175–187.
73. Martinez-Izquierdo,J. and Hohn,T. (1987) Cauliflower mosaic virus coat protein is phosphorylated in vitro by a virion-associated protein kinase. *Proc. Natl. Acad. Sci. U.S.A.*, **84**, 1824–1828.
74. Karsies,A., Hohn,T. and Leclerc,D. (2001) Degradation signals within both terminal domains of the cauliflower mosaic virus capsid protein precursor. *Plant J.*, **27**, 335–343.
75. Pfeiffer,P., Laquel,P. and Hohn,T. (1984) Cauliflower mosaic virus replication complexes: characterization of the associated enzymes and of the polarity of the DNA synthesized in vitro. *Plant Mol. Biol.*, **3**, 261–270.
76. Haseloff,J. and Siemering,K. (1998) The uses of green fluorescent protein in plants. In: Chalfie,M. and Kain,S. (eds). *Green Fluorescent Protein: Properties, Applications and Protocols*. Wiley-Liss, Inc., NY, pp. 191–220.
77. Hanson,M.R. and Köhler,R.H. (2001) GFP imaging: methodology and application to investigate cellular compartmentation in plants. *J. Exp. Bot.*, **52**, 529–539.
78. Champagne,J., Benhamou,N. and Leclerc,D. (2004) Localization of the N-terminal domain of cauliflower mosaic virus coat protein precursor. *Virology*, **324**, 257–262.
79. Kosugi,S., Hasebe,M., Tomita,M. and Yanagawa,H. (2009) Systematic identification of cell cycle-dependent yeast nucleocytoplasmic shuttling proteins by prediction of composite motifs. *Proc. Natl. Acad. Sci. U.S.A.*, **106**, 10171–10176.
80. Sperschneider,J., Catanzariti,A.-M., DeBoer,K., Petre,B., Gardiner,D.M., Singh,K.B., Dodds,P.N. and Taylor,J.M. (2017) LOCALIZER: subcellular localization prediction of both plant and effector proteins in the plant cell. *Sci. Rep.*, **7**, 44598.
81. Haas,G., Azevedo,J., Moissiard,G., Geldreich,A., Himber,C., Bureau,M., Fukuhara,T., Keller,M. and Voinnet,O. (2008) Nuclear import of CaMV P6 is required for infection and suppression of the RNA silencing factor DRB4. *EMBO J.*, **27**, 2102–2112.
82. Pooggin,M.M. and Ryabova,L.A. (2018) Ribosome shunting, polycistronic translation, and evasion of antiviral defenses in plant pararetroviruses and beyond. *Front. Microbiol.*, **9**, 644.
83. Hemmings-Mieszczak,M., Steger,G. and Hohn,T. (1997) Alternative structures of the cauliflower mosaic virus 35 S RNA leader: implications for viral expression and replication. *J. Mol. Biol.*, **267**, 1075–1088.
84. Hohn,T. and Rothnie,H. (2013) Plant pararetroviruses: replication and expression. *Curr. Opin. Virol.*, **3**, 621–628.
85. Guerra-Peraza,O., de Tapia,M., Hohn,T. and Hemmings-Mieszczak,M. (2000) Interaction of the cauliflower mosaic virus coat protein with the pregenomic RNA leader. *J. Virol.*, **74**, 2067–2072.
86. Pfeiffer,P. and Hohn,T. (1983) Involvement of reverse transcription in the replication of cauliflower mosaic virus: a detailed model and test of some aspects. *Cell*, **33**, 781–789.
87. Williams,B.J.L., Boyne,J.R., Goodwin,D.J., Roaden,L., Hautbergue,G.M., Wilson,S.A. and Whitehouse,A. (2005) The prototype gamma-2 herpesvirus nucleocytoplasmic shuttling protein, ORF 57, transports viral RNA through the cellular mRNA export pathway. *Biochem. J.*, **387**, 295–308.
88. Chaudhary,S., Khokhar,W., Jabre,I., Reddy,A.S.N., Byrne,L.J., Wilson,C.M. and Syed,N.H. (2019) Alternative splicing and protein diversity: plants versus animals. *Front. Plant Sci.*, **10**, 708.
89. Fütterer,J., Gordon,K., Bonneville,J.M., Sanfaçon,H., Pisan,B., Penswick,J. and Hohn,T. (1988) The leading sequence of caulimovirus large RNA can be folded into a large stem-loop structure. *Nucleic Acids Res.*, **16**, 8377–8390.
90. Zuker,M. (2003) Mfold web server for nucleic acid folding and hybridization prediction. *Nucleic Acids Res.*, **31**, 3406–3415.
91. Köhler,A. and Hurt,E. (2007) Exporting RNA from the nucleus to the cytoplasm. *Nat. Rev. Mol. Cell Biol.*, **8**, 761–773.
92. Pan,H., Liu,S. and Tang,D. (2012) HPR1, a component of the THO/TREX complex, plays an important role in disease resistance and senescence in Arabidopsis. *Plant J. Cell Mol. Biol.*, **69**, 831–843.
93. Xu,C., Zhou,X. and Wen,C.-K. (2015) HYPER RECOMBINATION1 of the THO/TREX complex plays a role in controlling transcription of the REVERSION-TO-ETHYLENE SENSITIVITY1 gene in Arabidopsis. *PLos Genet.*, **11**, e1004956.
94. Strässer,K. and Hurt,E. (2000) Yra1p, a conserved nuclear RNA-binding protein, interacts directly with Mex67p and is required for mRNA export. *EMBO J.*, **19**, 410–420.

95. Zenklusen,D., Vinciguerra,P., Strahm,Y. and Stutz,F. (2001) The yeast hnRNP-Like proteins Yra1p and Yra2p participate in mRNA export through interaction with Mex67p. *Mol. Cell. Biol.*, **21**, 4219–4232.
96. Kang,Y. and Cullen,B.R. (1999) The human Tap protein is a nuclear mRNA export factor that contains novel RNA-binding and nucleocytoplasmic transport sequences. *Genes Dev.*, **13**, 1126–1139.
97. Cullen,B.R. (2003) Nuclear RNA export. *J. Cell Sci.*, **116**, 587–597.
98. LeBlanc,J.J., Uddowla,S., Abraham,B., Clatterbuck,S. and Beemon,K.L. (2007) Tap and Dbp5, but not Gag, are involved in DR-mediated nuclear export of unspliced Rous sarcoma virus RNA. *Virology*, **363**, 376–386.
99. Sakuma,T., Davila,J.I., Malcolm,J.A., Kocher,J.-P.A., Tonne,J.M. and Ikeda,Y. (2014) Murine leukemia virus uses NXF1 for nuclear export of spliced and unspliced viral transcripts. *J. Virol.*, **88**, 4069–4082.
100. Pessel-Vivares,L., Houzet,L., Lainé,S. and Mougel,M. (2015) Insights into the nuclear export of murine leukemia virus intron-containing RNA. *RNA Biol.*, **12**, 942–949.
101. Mougel,M., Akkawi,C., Chamontin,C., Feuillard,J., Pessel-Vivares,L., Socol,M. and Laine,S. (2020) NXF1 and CRM1 nuclear export pathways orchestrate nuclear export, translation and packaging of murine leukaemia retrovirus unspliced RNA. *RNA Biol.*, **17**, 528–538.
102. Flint,S.J., Huang,W., Goodhouse,J. and Kyin,S. (2005) A peptide inhibitor of exportin1 blocks shuttling of the adenoviral E1B 55 kDa protein but not export of viral late mRNAs. *Virology*, **337**, 7–17.
103. Yatherajam,G., Huang,W. and Flint,S.J. (2011) Export of adenoviral late mRNA from the nucleus requires the Nxf1/Tap export receptor. *J. Virol.*, **85**, 1429–1438.
104. Johnson,L.A., Li,L. and Sandri-Goldin,R.M. (2009) The cellular RNA export receptor TAP/NXF1 is required for ICP27-mediated export of herpes simplex virus 1 RNA, but the TREX complex adaptor protein Aly/REF appears to be dispensable. *J. Virol.*, **83**, 6335–6346.
105. Tian,X., Devi-Rao,G., Golovanov,A.P. and Sandri-Goldin,R.M. (2013) The interaction of the cellular export adaptor protein Aly/REF with ICP27 contributes to the efficiency of herpes simplex virus 1 mRNA export. *J. Virol.*, **87**, 7210–7217.
106. Heise,T., Sommer,G., Reumann,K., Meyer,I., Will,H. and Schaal,H. (2006) The hepatitis B virus PRE contains a splicing regulatory element. *Nucleic Acids Res.*, **34**, 353–363.
107. Lee,G.H., Wasser,S. and Lim,S.G. (2008) Hepatitis B pregenomic RNA splicing—The products, the regulatory mechanisms and its biological significance. *Virus Res.*, **136**, 1–7.
108. Sommer,G. and Heise,T. (2008) Posttranscriptional control of HBV gene expression. *Front. Biosci. J. Virtual Libr.*, **13**, 5533–5547.
109. Hernandez,F.P. and Sandri-Goldin,R.M. (2010) Head-to-tail intramolecular interaction of herpes simplex virus type 1 regulatory protein ICP27 is important for its interaction with cellular mRNA export receptor TAP/NXF1. *mBio*, **1**, e00268-10.
110. Diot,C., Fournier,G., Dos Santos,M., Magnus,J., Komarova,A., van der Werf,S., Munier,S. and Naffakh,N. (2016) Influenza A virus polymerase recruits the RNA helicase DDX19 to promote the nuclear export of viral mRNAs. *Sci. Rep.*, **6**, 33763.
111. Ren,X., Yu,Y., Li,H., Huang,J., Zhou,A., Liu,S., Hu,P., Li,B., Qi,W. and Liao,M. (2019) Avian influenza A virus polymerase recruits cellular RNA helicase eIF4A3 to promote viral mRNA splicing and spliced mRNA nuclear export. *Front. Microbiol.*, **10**, 1625.
112. Marsh,L.E. and Guilfoyle,T.J. (1987) Cauliflower mosaic virus replication intermediates are encapsidated into virion-like particles. *Virology*, **161**, 129–137.
113. Himmelbach,A., Chapdelaine,Y. and Hohn,T. (1996) Interaction between cauliflower mosaic virus inclusion body protein and capsid protein: implications for viral assembly. *Virology*, **217**, 147–157.
114. Menissier,J., Laquel,P., Lebeurier,G. and Hirth,L. (1984) A DNA polymerase activity is associated with Cauliflower Mosaic Virus. *Nucleic Acids Res.*, **12**, 8769–8778.
115. Haas,M., Bureau,M., Geldreich,A., Yot,P. and Keller,M. (2002) Cauliflower mosaic virus: still in the news. *Mol. Plant Pathol.*, **3**, 419–429.
116. Kobayashi,K., Nakayashiki,H., Tsuge,S., Mise,K. and Furusawa,I. (1998) Accumulation kinetics of viral gene products in cauliflower mosaic virus-infected turnip protoplasts. *Microbiol. Immunol.*, **42**, 65–69.
117. Li,H.-C., Huang,E.-Y., Su,P.-Y., Wu,S.-Y., Yang,C.-C., Lin,Y.-S., Chang,W.-C. and Shih,C. (2010) Nuclear export and import of human hepatitis B virus capsid protein and particles. *PLoS Pathog.*, **6**, e1001162.